Original Article

Mixed local and ultra-distal volcanic ash deposition within the Upper Cretaceous Kanguk Formation, Sverdrup Basin, Canadian Arctic Islands

Michael A Pointon[1] , Michael J Flowerdew[1] , Peter Hülse[1] , Simon Schneider[1] and Martin J Whitehouse[2]

[1]CASP, West Building, Madingley Rise, Madingley Road, Cambridge, CB3 0UD, United Kingdom and [2]Department of Geosciences, Swedish Museum of Natural History, SE-104 05 Stockholm, Sweden

Abstract

The Upper Cretaceous Kanguk Formation of the Sverdrup Basin, Canadian Arctic Islands, contains numerous diagenetically altered volcanic ash layers (bentonites). Eleven bentonites were sampled from an outcrop section on Ellesmere Island for U–Pb zircon secondary ion mass spectrometry dating and whole-rock geochemical analysis. Two distinct types of bentonite are identified from the geochemical data. Relatively thick (0.1 to 5 m) peralkaline rhyolitic to trachytic bentonites erupted in an intraplate tectonic setting. These occur throughout the upper Turonian to lower Campanian (*c.* 92–83 Ma) outcrop section and are likely associated with the alkaline phase of the High Arctic Large Igneous Province. Two thinner (<5 cm) subalkaline dacitic to rhyolitic bentonites of late Turonian to early Coniacian age (*c.* 90–88 Ma) are also identified. The geochemistry of these bentonites is consistent with derivation from volcanoes within an active continental margin tectonic setting. The lack of nearby potential sources of subalkaline magmatism, together with the thinner bed thickness of the subalkaline bentonites and the small size of zircon phenocrysts therein (typically 50–80 μm in length) are consistent with a more distal source area. The zircon U–Pb age and whole-rock geochemistry of these two subalkaline bentonites correlate with an interval of intense volcanism in the Okhotsk–Chukotka Volcanic Belt, Russia. It is proposed that during late Turonian to early Coniacian times intense volcanism within the Okhotsk–Chukotka Volcanic Belt resulted in widespread volcanic ash dispersal across Arctic Alaska and Canada, reaching as far east as the Sverdrup Basin, more than 3000 km away.

1. Introduction

The Upper Cretaceous Kanguk Formation within the Sverdrup Basin, Arctic Canada (Fig. 1), contains an important record of Late Cretaceous volcanism within the Arctic realm, which can provide insights into the opening of the Arctic Ocean and the tempo of volcanism associated with the late stages of the High Arctic Large Igneous Province (HALIP; e.g. Davis *et al.* 2016). The record is manifest as numerous diagenetically altered volcanic ash layers (bentonites), which have been reported from several localities within the basin (e.g. Pugh *et al.* 2014; Schröder-Adams *et al.* 2014; Davis *et al.* 2016; Davies *et al.* 2018). The bentonites are dominated by clay minerals, but also contain trace amounts of volcanic phenocrysts, some of which are amenable to isotopic dating. For example, zircon phenocrysts separated from several Kanguk Formation bentonites sampled from two sections towards the basin centre have been dated recently using the U–Pb chemical abrasion isotope dilution thermal ionization mass spectrometry (CA-ID-TIMS) method (Davis *et al.* 2016; Fig. 1). These yielded precise late Cenomanian to early Campanian ages, constraining the eruption ages of the bentonites and the stratigraphic age range of the enveloping Kanguk Formation.

Whilst the age range of the Kanguk Formation bentonites is comparatively well known, the location of their source volcanoes is more poorly constrained. This is in part because fine-grained tephra from explosive volcanic eruptions can be carried by wind over considerable distances. The extensively altered mineralogy of the bentonites provides little insight into their original volcanic composition, although whole-rock geochemical analysis has been demonstrated in studies of bentonites elsewhere to be more informative (e.g. Huff *et al.* 1993; Parsons, 1994; Christidis *et al.* 1995; Spears *et al.* 1999). The major elements, which are routinely used to classify fresh or slightly altered volcanic rocks, are of limited use when classifying extensively altered volcanic rocks because several elements, including K and Na, are known to be mobile during weathering and diagenesis (Winchester & Floyd, 1977; Floyd & Winchester, 1978; Zielinski, 1982; Christidis, 1998). Instead, the analysis of altered volcanic
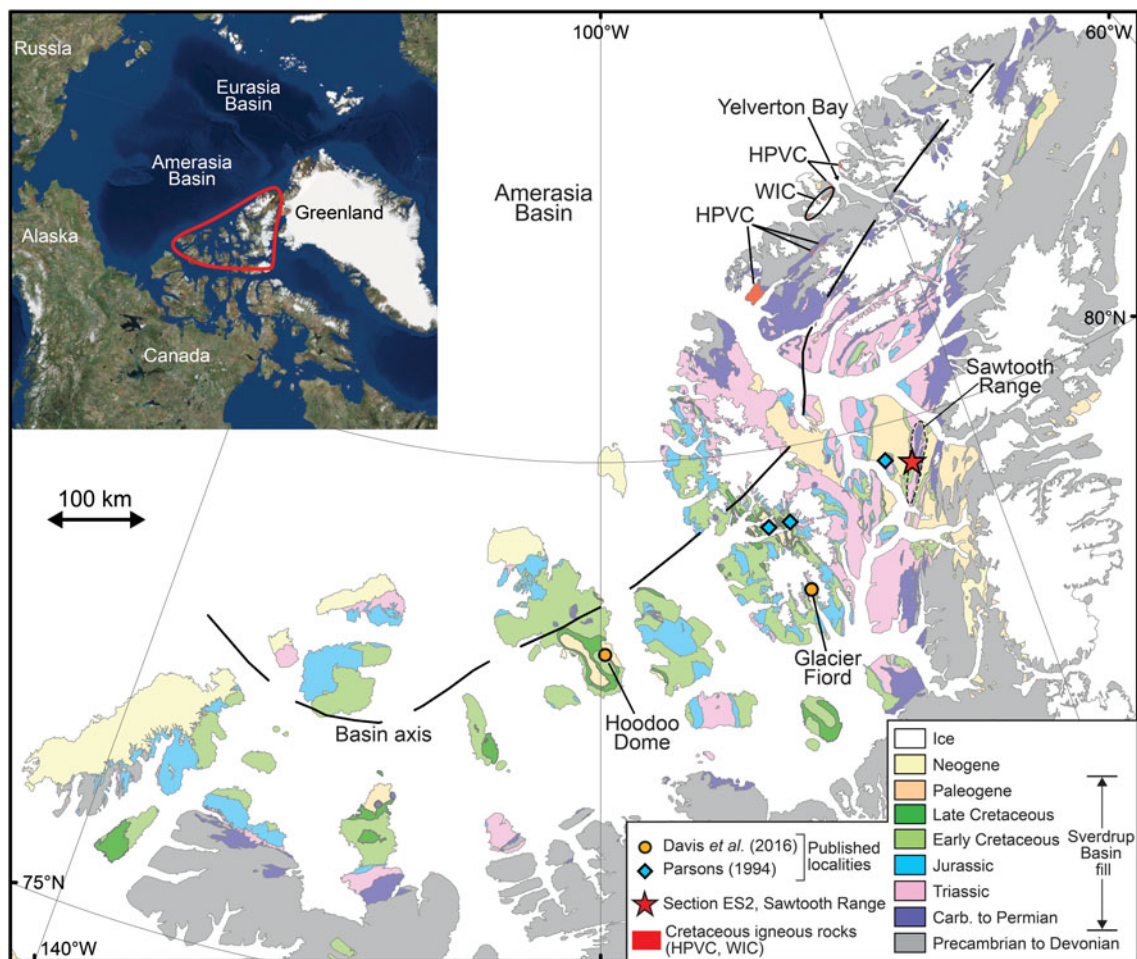
Fig. 1. (Colour online) Geological map of the Sverdrup Basin showing the location of section ES2 within the Sawtooth Range, Ellesmere Island. The map is simplified from Harrison *et al.* (2011). Basin axis is redrawn from Embry & Beauchamp (2008). HPVC – Hansen Point Volcanic Complex; WIC – Wootton Intrusive Complex. The inset map shows the approximate area of the Arctic covered by the main figure.

rocks focuses on trace elements including Ti, Zr, Nb, Hf and Ta, which are generally considered to be immobile during most upper crustal processes and are also indicators of petrogenetic processes (Floyd & Winchester, 1978; Huff *et al.* 1993; Kiipli *et al.* 2017). Presently, however, there is a dearth of published geochemical data from the Kanguk Formation bentonites. Parsons (1994) investigated the geochemistry and petrogenesis of 12 Kanguk Formation bentonites from three outcrop sections (Fig. 1), inferring a volcanic source area along the Sverdrup Rim, on northern Ellesmere Island and/or on northern Greenland. This dataset, however, includes only a small proportion of the total number of bentonites within the formation.

In addition to elucidating Late Cretaceous tectonic and magmatic events within the Arctic region, identifying the source(s) of bentonites within the Kanguk Formation has the potential to help constrain the regional geographic and stratigraphic distribution of volcanic ash. This may aid in the identification of coeval bentonites beyond the Sverdrup Basin. Through geochemical fingerprinting and isotopic dating techniques, bentonites can provide a robust basis for regional stratigraphic correlation (e.g. Inanli *et al.* 2009; Kiipli *et al.* 2011, 2013, 2015; Sell *et al.* 2015). Ultimately, this may lead to more precise regional stratigraphic correlations along the Arctic Alaska–Canada continental margin and offshore within the Amerasia Basin.

To constrain better the volcanic sources of the Kanguk Formation bentonites, whole-rock geochemical analyses were performed on 11 bentonites sampled from an outcrop section in the Sawtooth Range, Fosheim Peninsula, Ellesmere Island (Fig. 1). U–Pb zircon secondary ion mass spectrometry (SIMS) dating of five of these bentonites was also undertaken to provide absolute age constraints on the sampled section and the bentonites investigated.

2. Geological setting

2.a. Sverdrup Basin

The Sverdrup Basin covers an area of ~300,000 km² and contains up to 13 km of Carboniferous to Eocene sedimentary strata (Embry & Beauchamp, 2008; Fig. 1). It developed as a rift basin on Siluro-Devonian rocks of the Franklinian Mobile Belt (Hadlari *et al.* 2016). The Amerasia Basin borders the basin to the north (Fig. 1). The eastern parts of the Sverdrup Basin, including Ellesmere and Axel Heiberg islands, were deformed during Palaeogene times as part of the Eurekan Orogeny (Piepjohn *et al.* 2016).

The stratigraphy of the Sverdrup Basin was divided into eight major depositional phases by Embry & Beauchamp (2008). These are characterized by distinct tectonic and depositional regimes, and are bounded by unconformities (Fig. 2). The three youngest phases
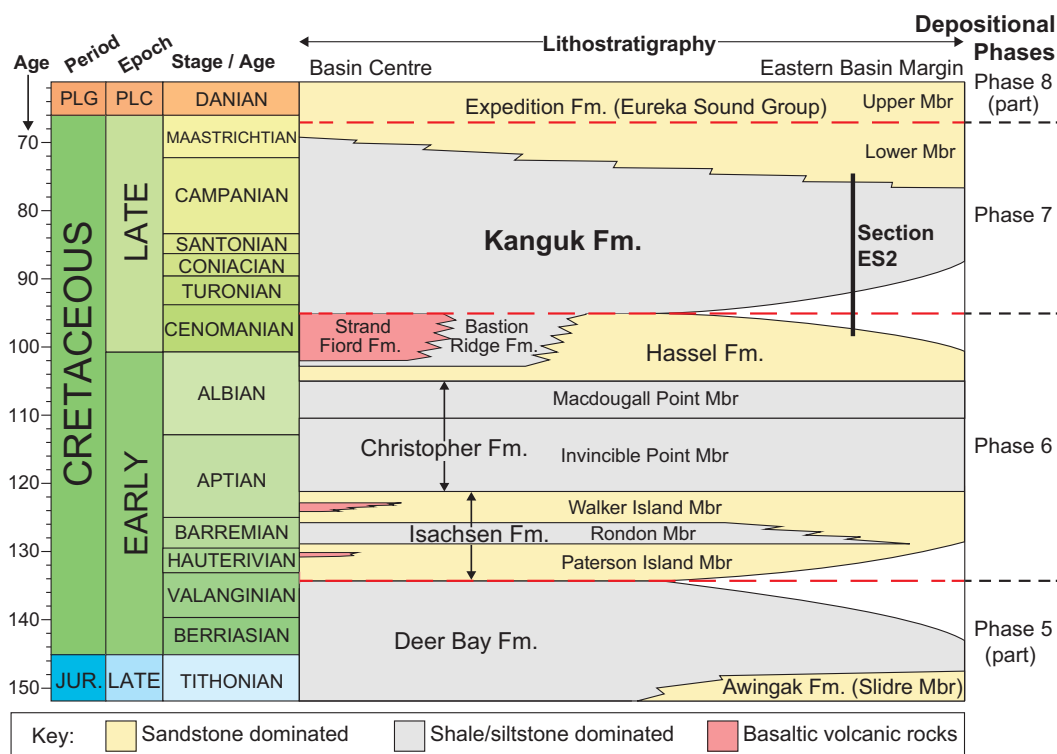
Fig. 2. (Colour online) Cretaceous lithostratigraphic framework of the Sverdrup Basin (after Embry & Osadetz, 1988; Embry, 1991). The top of the Kanguk Formation is drawn according to Ricketts (1991). Lithostratigraphic unit abbreviations: Fm. – formation; Mbr – member. The timescale shown follows Cohen *et al.* (2013). The red dashed lines represent unconformities or paraconformities. Depositional phases are drawn after Embry & Beauchamp (2008). PLG – Paleogene; PLC – Paleocene.

(six to eight) are relevant to the present study and are summarized below:

Phase six commenced in late Valanginian times with a marked increase in subsidence and sediment supply rates, linked to rifting and extension. Thick, coarse-grained fluvio-deltaic siliciclastic sediments, sourced from the south and east, were deposited across a large area of the basin (Isachsen Formation; Fig. 2; Embry, 1991; Tullius *et al.* 2014). Towards the northeast of the basin, on northern Ellesmere and Axel Heiberg islands, basaltic flows and pyroclastic rocks occur interbedded with these sediments (Fig. 2; Embry & Osadetz, 1988; Embry, 1991). These volcanic deposits thicken northwards (Embry, 1991). A major transgression in middle Aptian times led to the deposition of marine mudstones and siltstones assigned to the Christopher Formation. Towards the end of phase six (late Albian to Cenomanian) fluvio-deltaic to shallow shelfal sands of the Hassel Formation prograded into the basin. In the basin centre, intense volcanism produced thick, mainly subaerial, tholeiitic basaltic flows that characterize the Strand Fiord Formation (Ricketts *et al.* 1985; Estrada & Henjes-Kunst, 2004). These have an inferred late Albian to Cenomanian age (Embry, 1991) based on several whole-rock $^{40}Ar–^{39}Ar$ dates of 103–95 Ma (Tarduno *et al.* 1998; Villeneuve & Williamson, 2006; Estrada & Henjes-Kunst, 2013) and a late Albian palynomorph assemblage recovered from intercalated siliciclastic rocks (Núñez-Betelu *et al.* 1994). Lava flows thicken towards the north and have been inferred to represent the cratonward extension of the Alpha Ridge in the Amerasia Basin (Ricketts *et al.* 1985) and to form part of the HALIP (e.g. Saumur *et al.* 2016; Dostal & MacRae, 2018; Kingsbury *et al.* 2018).

Phase seven started in late Cenomanian times and was characterized by tectonic quiescence and slow subsidence. Its onset correlates with a major transgression leading to the deposition of the

shales and silts of the Kanguk Formation across a large area of the basin (Embry, 1991; Schröder-Adams *et al.* 2014). Towards the end of Late Cretaceous times, sediment input rates increased and shoreline to shallow marine sandstones prograded into the basin from the east (Lower Member of the Expedition Formation; Fig. 2). Widespread uplift marked the end of this phase.

Phase eight marked a transition from thermally dominated subsidence to compressional loading caused by convergence between Greenland and Arctic Canada (Eurekan Orogeny). Eastern parts of the basin underwent rapid subsidence and were loci for the deposition of fluvio-deltaic sediments (Upper Member of the Expedition Formation to Iceberg Bay Formation; Ricketts, 1986, 1991, 1994). These are overlain by lower to middle Eocene syntectonic conglomerates deposited in more restricted intermontane basins (Buchanan Lake Formation; Ricketts, 1994). During late Eocene times, Eurekan deformation climaxed, the entire basin was uplifted and deposition within the Sverdrup Basin ended.

2.b. Kanguk Formation

The Kanguk Formation is a mudstone-dominated marine unit containing minor interbedded siltstone, sandstone and bentonite horizons. In the type section, located on Kanguk Peninsula, western Axel Heiberg Island, the base of the Kanguk Formation is defined by a sharp transition from the underlying volcanic rocks of the Strand Fiord Formation (Fig. 2; Souther, 1963; Tozer, 1963). Beyond Axel Heiberg Island, however, the Kanguk Formation usually overlies fluvio-deltaic to marine shelf sandstones of the Hassel Formation with a sharp contact, representing an unconformity or paraconformity (Fig. 2). In the type section, the top of the Kanguk Formation was originally placed beneath the first major sandstone bed. Inconsistent application of this definition prompted Ricketts

(1991) to revise the top of the Kanguk Formation to the level where sandstone beds make up 40 % of the section. In several areas of the basin, the Kanguk Formation has been subdivided into between two and five informal members (e.g. Fricker, 1963, p. 119; Balkwill & Hopkins, 1976; Davies *et al.* 2018). In the studied section, Davies *et al.* (2018) subdivided the Kanguk Formation into two informal members: a lower member dominated by dark grey shales (with minor silty intervals; 84 m thick) and an upper member comprising rusty-brown to dark grey shales and mudstones with concretions (~65 m exposed, up to 25 m covered; Fig. 3).

Beyond the Sverdrup Basin, the Kanguk Formation has been correlated with the Boundary Creek and Smoking Hills formations in the Mackenzie Delta area, and the Canning Formation, Hue Shale and Seabee Formation in Northern Alaska (Embry & Dixon, 1990; Pugh *et al.* 2014). The Kanguk Formation has also been identified as a potential, albeit thermally immature, regional source rock for hydrocarbons in the Sverdrup Basin (Houseknecht & Bird, 2011).

The thickness of the Kanguk Formation ranges from less than 150 m at the eastern basin margin to more than 750 m at the basin centre (Embry, 1991). In the type section, a total thickness of ~250 m was reported by Souther (1963). In this area, the lower portion of the Kanguk Formation typically consists of black, bituminous, papery shales, interpreted to represent starved, offshore shelf deposits (Embry, 1991). In general, the shales of the formation become siltier, lighter in colour and less bituminous up stratigraphy; the upper portion of the formation consists mainly of pro-deltaic deposits (Embry, 1991). In more marginal sections, like the one investigated as part of this study, coarser-grained units (up to medium-grained sand) are observed in the lower part of the formation and are interpreted to represent shallow marine shelf deposits (Embry, 1991).

The Kanguk Formation has been the focus of intense biostratigraphic investigation, studying various fossil groups including palynomorphs (e.g. Núñez-Betelu *et al.* 1994; Nunez-Betelu & Hills, 1994; Lenniger *et al.* 2014), diatoms (Tapia & Harwood, 2002; Witkowski *et al.* 2011), radiolarians (Pugh *et al.* 2014), foraminifers (Schröder-Adams *et al.* 2014), ammonites (e.g. Jeletzky, 1970) and vertebrates (Tarduno *et al.* 1998; Vavrek *et al.* 2014; Bono *et al.* 2016). Collectively, these suggest a late Cenomanian to Maastrichtian age range for the Kanguk Formation at the basin centre (*c.* 97–66 Ma; Fig. 2). U–Pb zircon CA-ID-TIMS dates from bentonites within the Kanguk and Bastion Ridge formations (Davis *et al.* 2016) support a late Cenomanian to early Campanian age range for the Kanguk Formation on Axel Heiberg Island. Moreover, chemostratigraphic investigations employing stable carbon isotopes have identified a positive isotopic excursion in the basal Kanguk Formation, which has been interpreted to record the late Cenomanian to early Turonian oceanic anoxic event two (OAE2) in the High Arctic (Lenniger *et al.* 2014; Pugh *et al.* 2014; Schröder-Adams *et al.* 2014; Herrle *et al.* 2015).

3. Materials and methods

3.a. Bentonite samples

Eleven bentonite samples were collected from a river section in the Sawtooth Range, Fosheim Peninsula, central Ellesmere Island (section ES2; Fig. 1). The section is from near the eastern margin
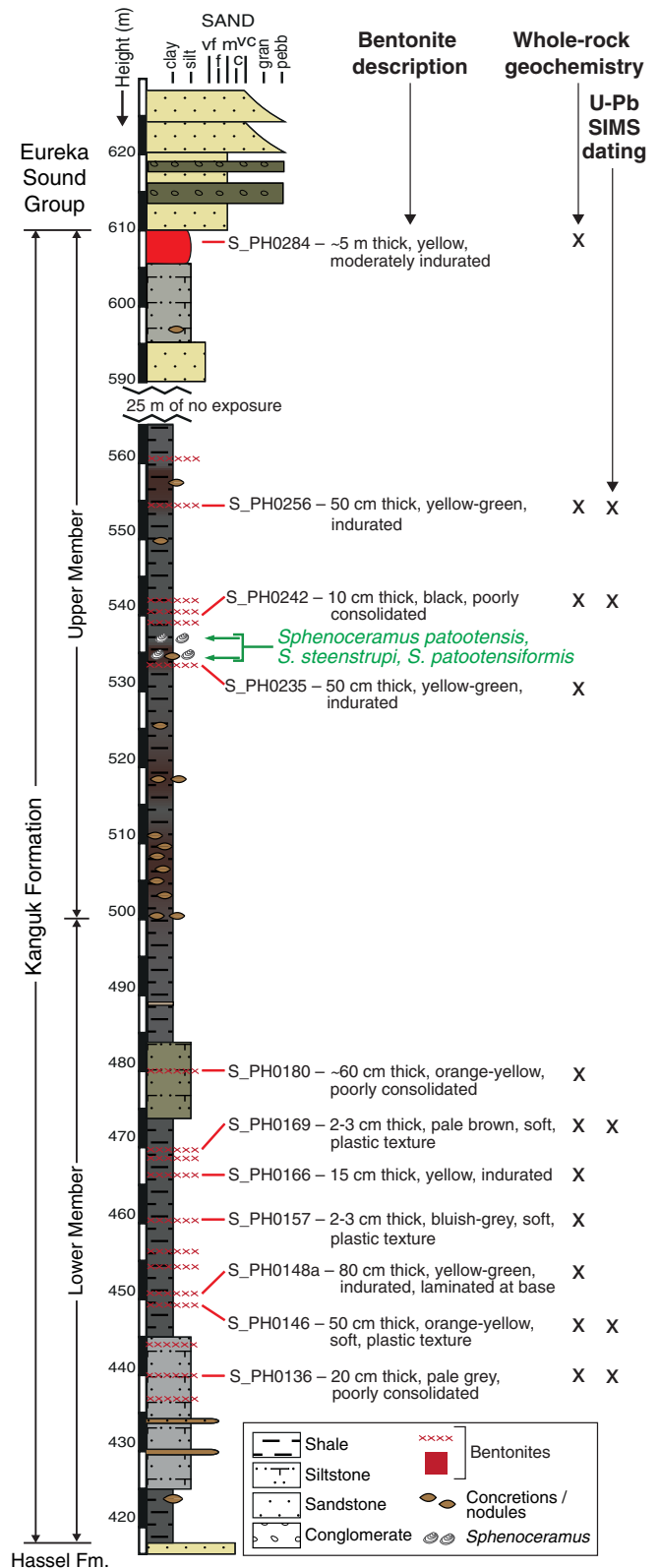
Fig. 3. (Colour online) Lithological log showing the section heights of bentonite samples and analyses undertaken. Bentonite grain size is not drawn to scale. Colour in the sedimentary column approximately reflects rock colour. This is apart from the bentonites whose colours are described in the bentonite descriptions. Note there is a gap of 25 m in the section at 565–590 m. Informal members of the Kanguk Formation are drawn following Davies *et al.* (2018).
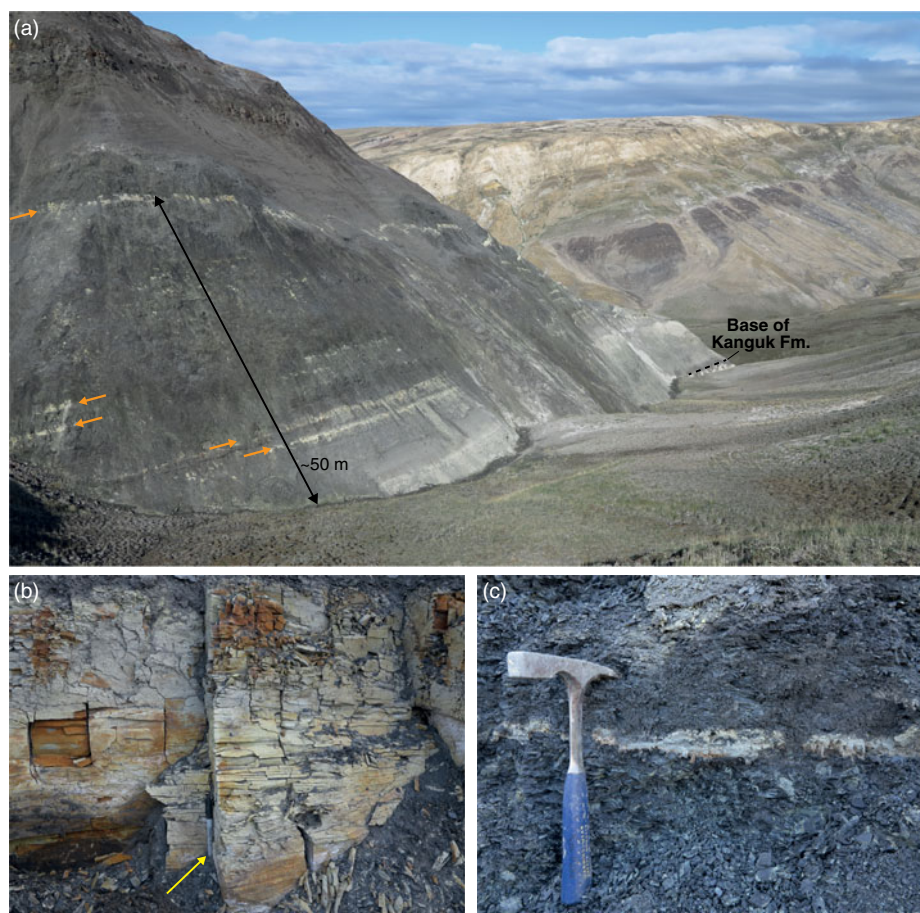
Fig. 4. (Colour online) Field photographs of Kanguk Formation bentonites. (a) The lower part of the sampled section. Thicker bentonite horizons can be seen from a distance weathering out of the section (indicated by orange arrows). (b) Bentonite S_PH0152. The marker pen for scale is 13.5 cm long (indicated by a yellow arrow). (c) Bentonite S_PH0169. The hammer for scale is 30 cm long.

of the basin (Fig. 1). At this locality the Kanguk Formation is ~195 m thick (Fig. 3) and comprises predominantly dark grey to black shales and siltstones (Figs. 3, 4a). In general, the shales are darker and finer grained in the lower part of the succession. Yellow weathering, fine- to coarse-grained, fining upwards sandstone beds are common and typically overlie siltstones or shales with a sharp base. Centimetre to decimetre thick bentonites and volcanic ash beds are intercalated throughout the succession and are heterogeneously distributed: up to 12 horizons were observed in the lower part of the Kanguk Formation and fewer (up to seven) horizons in the middle and upper parts of the formation (Fig. 3). The bentonite horizons vary in thickness; apart from a 5 m thick horizon towards the top of the section (Fig. 3), the bentonites are ~2 to 80 cm thick. They display a range of colours from bluish grey to orange (Figs. 3, 4). Some bentonites are indurated, whereas others are poorly consolidated and possess soft, plastic textures.

X-ray diffraction (XRD) analysis of whole-rock samples reveals that the bentonites have similar bulk mineralogy and that the samples are dominated by poorly crystalline phases (Fig. 5). In most samples there is a prominent mixed-layer clay peak (7–8 °2θ; Fig. 5), although the composition of the mixed-layer clay cannot be determined without further XRD analysis of the clay-sized fraction. In several bentonite samples there is a prominent broad peak at ~22 °2θ, which is characteristic of microcrystalline
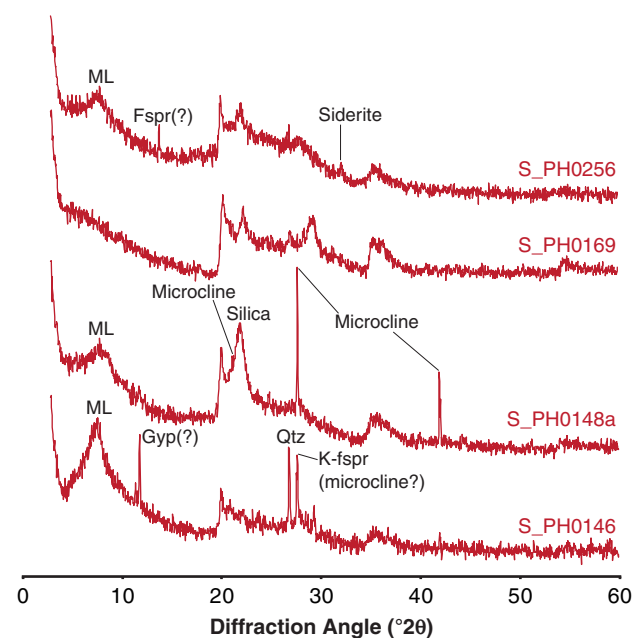
Fig. 5. (Colour online) Representative whole-rock X-ray diffraction traces. Fspr – feldspar; Gyp – gypsum; ML – mixed-layer clay; Qtz – quartz.

silica (e.g. S_PH0148a; Fig. 5). The lowest four bentonites analysed (S_PH0136, 0146, 0148a, 0152) all contain a number of tight peaks, which are indicative of highly crystalline phases. Some of these peaks correspond with quartz and feldspar (probably microcline; Fig. 5). These peaks may record the occurrence of relict igneous phenocrysts, as quartz and K-feldspar phenocrysts have been recovered from Kanguk bentonites sampled elsewhere on Ellesmere and Axel Heiberg islands (Parsons, 1994).

Zircon was recovered from 6 of the 11 bentonites (S_PH0136, 0146, 0157, 0169, 0242 and 0256). It is notably more abundant and of larger average grain size (up to 200 μm in length) in bentonites S_PH0136 and S_PH0146, from the base of the section (Fig. 3). In addition to euhedral zircon, several of the bentonite samples contain euhedral apatite, pyrite and a red-brown opaque mineral (possibly ilmenite). Similar restricted heavy mineral assemblages have been interpreted to be indicative of primary bentonites; that is, those formed through the *in situ* alteration of volcanic ash (Weaver, 1963).

3.b. U–Pb zircon SIMS geochronology

Approximately 300–500 g of each bentonite sample was processed for zircon separation. Most of the bentonite samples were disaggregated using a steel jaw crusher. This is with the exception of poorly consolidated samples, which were disaggregated by hand using an agate mortar and pestle. Samples were sieved using a 250 μm sieve and the <250 μm fraction was processed for zircon separation. Samples were washed several times in water to remove the clay fractions and were then dried in an oven. Zircons were concentrated using standard methods; that is, heavy liquid separation using LST (ρ = 2.8 g cm^{-3}), followed by magnetic separation.

Zircons were hand-picked using a binocular microscope onto double-sided sticky tape. Sample grains, together with fragments of the 91500 zircon standard (Wiedenbeck *et al.* 1995), were then mounted in epoxy at the NORDSIM facility, Swedish Natural History Museum. The mount was polished to expose grain interiors before optical and scanning electron microscope cathodoluminescence (SEM-CL) imaging. When imaged under SEM-CL, most grains show fine growth and/or sector zonation. A few grains from bentonites S_PH0136, S_PH0146 and S_PH0256 appear to contain inherited cores, although where it was possible to analyse both the core and rim of a grain, these were indistinguishable in age within analytical uncertainties.

U–Pb geochronology was undertaken on sample zircon grains using the CAMECA 1280-IMS secondary ion mass spectrometer at the NORDSIM facility. Analytical protocols follow those of Whitehouse & Kamber (2005) and Jeon & Whitehouse (2015). A spot size of ~20 μm was used throughout. Analysis pits are ~2–3 μm deep; such shallow pits mean analyses correspond well with the SEM-CL images, which sample up to ~5 μm below the surface of a zircon grain. U–Pb isotope data from individual spot analyses were calculated on the basis of 12 measured ratios. All data were collected during a single ~24 hour analytical session in 2014. The 91500 zircon standard (Wiedenbeck *et al.* 1995) was used as the primary standard and was analysed every 4–6 sample analyses. A Pb/UO–UO$_2$/UO calibration scheme was used (Jeon & Whitehouse, 2015). The uncertainty of the U–Pb standard calibration was ±1.36 % (2SE; from 21 spot analyses) and this is propagated into the analytical uncertainties. No secondary standard zircon was analysed during the analytical session; however, long-term analysis of the TEMORA-2 zircon as an unknown has yielded a mean ^{206}Pb–^{238}U date of 418.0 ± 3.4 Ma (2SD; Jeon & Whitehouse, 2015), which agrees well with the accepted

date of 416.8 Ma (Black *et al.* 2004). U–Pb ages were calculated using the decay constants of Jaffey *et al.* (1971) and a natural ^{238}U/^{235}U ratio of 137.88, as recommended by Steiger & Jäger (1977). U–Pb Tera-Wasserburg concordia diagrams were drawn from data uncorrected for non-radiogenic (common) lead using Isoplot v. 4.15 (Ludwig, 2012). ^{207}Pb-corrected ages were calculated attributing all common lead to surficial contamination and corrected using a modern-day average terrestrial common Pb composition (^{207}Pb/^{206}Pb = 0.836; Stacey & Kramers, 1975). Five analyses contain no measurable common lead; these analyses are clearly labelled in online Supplementary Material Table S1. TuffZirc dates were calculated from the ^{207}Pb-corrected dates, and uncorrected ^{206}Pb–^{238}U dates for analyses containing no common lead, using Isoplot v. 4.15 (Ludwig, 2012). These are used to approximate the eruption ages of the bentonite horizons. A complete data table can be found in the online Supplementary Material.

3.c. Whole-rock geochemistry

Approximately 50 g of each bentonite sample were dried overnight at 105 °C and then comminuted to powders using a Resch planetary ball mill equipped with agate grinding vessels. Whole-rock bentonite powders were analysed for major-, trace- and rare earth element (REE) concentrations at ALS Minerals, Loughrea, Ireland, using their ME-MS81d method. The method involves fusing 0.2–0.4 g of powdered sample with lithium metaborate at 1000 °C, followed by HCl-HNO$_3$ acid digestion.

Major-element concentrations were determined using inductively coupled plasma atomic emission spectroscopy (ICP-AES). Trace and REE concentrations were determined using inductively coupled plasma mass spectrometry (ICP-MS). Loss-on-ignition (LOI) values range between 6.8 and 21.0 %, although excluding samples S_PH0157 and S_PH0169, LOI values are <10 %. Raw data are presented in online Supplementary Material Table S2.

4. Results

4.a. U–Pb SIMS geochronology

U–Pb SIMS geochronology was undertaken on zircon grains separated from five Kanguk Formation bentonites (Fig. 3). Fifteen spot analyses were undertaken on 13 grains from bentonite S_PH0136 and yielded concordant to slightly discordant dates (Fig. 6a). One concordant analysis is resolvably older than all other analyses (136/4.1; Fig. 6a). This is tentatively interpreted to represent an older inherited magmatic grain. Likewise, one analysis yielded younger U–Pb ages than all other analyses and is tentatively interpreted to have been affected by lead loss (136/5.1; Fig. 6a). The TuffZirc algorithm excludes these two analyses and yields a date of 90.4 $^{+1.0}/_{-0.8}$ Ma (97.8 % confidence, n = 13), which is interpreted as the preferred age of this bentonite.

Twenty-three spot analyses were undertaken on 18 grains from bentonite S_PH0146. These analyses comprise a dominant age population at *c.* 91.5 Ma and four older discordant analyses (Fig. 6b). Three of the discordant older analyses form a linear trend that is consistent with common lead contamination (Fig. 6b). Analysis 146/13.1 lies above this trend and likely contains an element of lead loss. Within the main age cluster, there is one slightly discordant analysis from an inherited core that yielded an older ^{207}Pb-corrected date of 94.4 Ma (146/7.2 Fig. 6b inset). The TuffZirc algorithm excluded analyses 146/7.2 and 146/13.1, together with analysis 146/7.1, which has an imprecise ^{207}Pb-corrected date, and analyses 146/4.1 and 146/6.1, which have relatively young ^{207}Pb-corrected
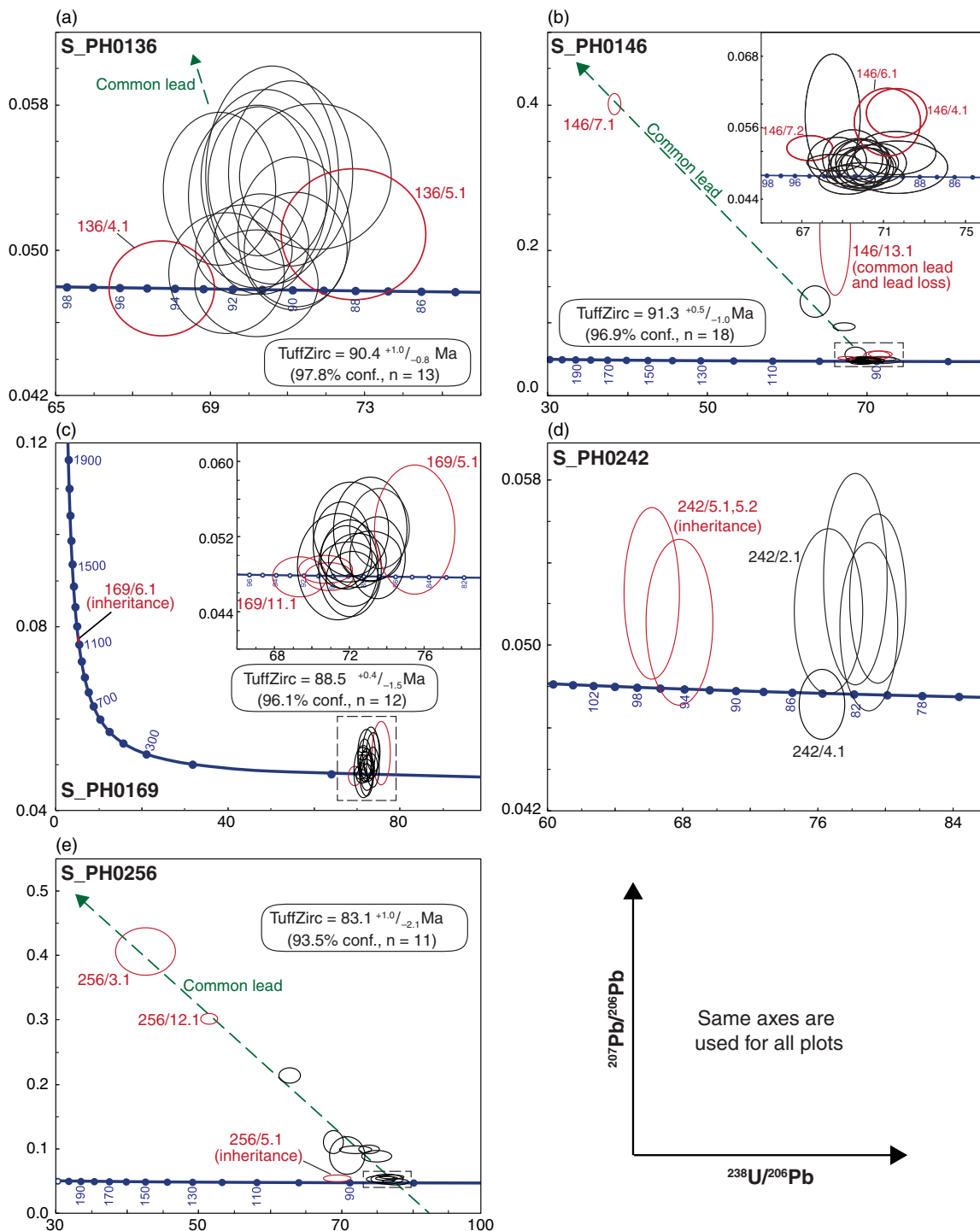
Fig. 6. (Colour online) Tera-Wasserburg U–Pb concordia diagrams showing U–Pb SIMS data from the Kanguk Formation bentonites. Uncertainty ellipses are drawn at the 2s confidence level; data are uncorrected for common lead. The blue band is the Concordia curve; blue numbers are concordant ages in units of Ma. Quoted dates are TuffZirc dates; black and red uncertainty ellipses denote analyses included/excluded by the TuffZirc algorithm.

dates. The remaining 18 analyses give a TuffZirc date of 91.3 $^{+0.5}/_{-1.0}$ Ma (96.9 % confidence). This is taken as the preferred age for bentonite S_PH0146.

Seventeen spot analyses were undertaken on 11 grains from bentonite S_PH0169. One grain yielded a substantially older concordant ^{207}Pb–^{206}Pb date of 1134 ± 15 Ma (169/6.1; Fig. 6c) and is interpreted as an inherited grain, either entrained during eruption,

or washed or blown in after deposition. On closer inspection of the data, two analyses only marginally overlap within uncertainty with the main sample age population (Fig. 6c inset) and are tentatively interpreted as another inherited grain (169/11.1) and a grain that has experienced minor lead loss (169/5.1), respectively. The TuffZirc algorithm excluded these three analyses, together with analyses 169/1.2 and 169/2.2, which have >90 Ma ^{207}Pb-corrected

dates. The remaining 12 analyses yield a TuffZirc date of 88.5 $^{+0.4}/_{-1.5}$ Ma (96.1 % confidence).

Owing to the poor recovery of zircon from bentonite S_PH0242, only eight spot analyses on five grains were undertaken. One analysis (242/3.1) yielded imprecise dates and contains substantial common lead. The other seven analyses form two concordant to slightly discordant age clusters at *c.* 96 and 82 Ma (Fig. 6d). The two *c.* 96 Ma analyses are from an anhedral, sector-zoned grain fragment, which is interpreted as an older inherited grain (242/5.1, 5.2; Fig. 6d). The younger, *c.* 82 Ma age cluster comprises three analyses from a single grain, which yielded 80–81 Ma ^{207}Pb-corrected dates (242/1.1–242/1.3), and single analyses from two grains, which yielded 83.2 and 84.1 Ma ^{207}Pb-corrected dates (242/2.1 and 242/4.1, respectively). These data are too scattered to represent a single age population. Their interpretation is, however, not straightforward. Supporting information, such as SEM-CL images and Th/U ratios, provide little insight: all grains are euhedral, contain fine-scale oscillatory zonation and have similar Th/U ratios (0.33–0.61). Given the uncertainty in the interpretation of these data, no eruption age is calculated for this sample.

Fourteen spot analyses were undertaken on 13 grains from bentonite S_PH0256. One analysis yielded relatively old, slightly discordant dates that do not overlap with the other analyses (256/5.1; Fig. 6e). This likely represents an inherited grain as there is no evidence for a xenocrystic core within this grain based on SEM-CL imaging. All remaining analyses yielded discordant to concordant dates that fall on a linear trend consistent with common lead contamination (Fig. 6e). The TuffZirc algorithm excludes analysis 256/5.1, together with analyses 256/3.1 and 256/12.1, which have imprecise ^{207}Pb-corrected dates. The remaining 11 analyses yield a TuffZirc date of 83.1 $^{+1.0}/_{-2.1}$ Ma (93.5 % confidence), which is taken as the preferred age of this bentonite.

4.b. Whole-rock geochemistry

Eleven bentonites were analysed for whole-rock geochemistry. These all show consistently greater enrichment in large-ion lithophile elements compared to the high field strength and REEs when data are normalized to primitive mantle values (Fig. 7a). Two bentonites, S_PH0157 and S_PH0169, exhibit negative Nb–Ta anomalies, which are conspicuously absent from the other bentonites analysed (Fig. 7a). Samples show similar trends in REE concentrations: chondrite-normalized REE trends are characterized by a stronger enrichment in light rare earth elements (LREE) than heavy rare earth elements (HREE) and negative europium anomalies (Fig. 7b). Bentonites S_PH0157 and S_PH0169 have smaller europium anomalies (0.51 and 0.38, respectively) than the other bentonites analysed (0.2–0.31).

As discussed in the introduction, the major elements (Si, Al, Na, K, Mg, Ca and Fe) are of limited use for classifying extensively altered volcanic rocks such as bentonites because of element mobility. Instead, the classification of altered volcanic rocks relies on several trace elements that are generally considered to be immobile during most upper crustal processes and are also indicators of petrogenetic processes. These include Ti, Zr, Nb, Hf and Ta (Winchester & Floyd, 1977; Huff *et al.* 1993; Kiipli *et al.* 2017). In felsic igneous rocks, the trace-element budget is commonly controlled by accessory minerals (Wark & Miller, 1993; Bea, 1996; Hoskin *et al.* 2000; Claiborne *et al.* 2010). These include apatite and zircon, which are ubiquitous phenocrysts in the Kanguk Formation bentonites.

Classification and tectonic discrimination diagrams are widely used in geochemical studies of bentonites to elucidate original (unaltered) ash compositions and the tectonic settings of the source volcanoes where direct petrogenetic and geological constraints are not available. Their usage is, however, controversial. This is because many diagrams employ absolute elemental concentrations, which are difficult to apply to bentonites because diagenetic alteration may render elemental abundances dissimilar to those of the original unaltered volcanic ash (e.g. through residual enrichment or element mobility). Furthermore, concerns have been raised about the efficacy of several widely used classification and tectonic discrimination diagrams developed during the 1970 s and 1980 s (e.g. Wang & Glover, 1992; Snow, 2006; Li *et al.* 2015). This is because such diagrams were constructed using limited datasets that under-represent the extent of geochemical variation in igneous rocks from different tectonic settings. Thus, caution should be exercised when using classification and discrimination diagrams in isolation, particularly for ancient altered volcanic rocks whose source cannot be established from direct field evidence.

On the Zr/TiO$_2$ versus Nb/Y classification diagram of Winchester & Floyd (1977) most of the bentonites plot in the comendite/pantellerite (peralkaline rhyolite) and trachyte fields. This is with the exception of bentonites S_PH0157 and S_PH0169, which plot within the subalkaline rhyolite and rhyodacite/dacite fields (Fig. 8a). Yttrium can sometimes be mobilized during the alteration of volcanic rocks to bentonites (e.g. Christidis, 1998; Hill *et al.* 2000). Thus, the measured Nb/Y ratios should be regarded as maximum estimates for the alkalinity of the original ash layers. Using the tectonic discrimination diagrams of Schandl & Gorton (2002) that employ ratios of Hf, Ta, Th and Yb, and are designed to identify the tectonic environments of felsic and intermediate volcanic rocks, all but two of the Kanguk Formation bentonites plot as a tight cluster in the within-plate volcanic zone field (Fig. 8b, c). Bentonites S_PH0157 and S_PH0169 plot separately, within the active continental margin field (Fig. 8b, c).

5. Discussion

5.a. U–Pb geochronology

U–Pb SIMS dating was undertaken on zircons separated from five Kanguk Formation bentonites. Four of these bentonites yielded robust ages, which are summarized in Table 1. In detail, the U–Pb age from bentonite S_PH0136 is slightly younger than that from the overlying bentonite S_PH0146 (Fig. 9; Table 1), although these ages are indistinguishable within analytical uncertainties.

The positions of chronostratigraphic stage boundaries within the studied section have been estimated through interpolation using the Bayesian chronological modelling software program OXCAL (Fig. 9; Bronk Ramsey, 2008; Bronk Ramsey & Lee, 2013). From the same OXCAL interpolation model, the age of an undated bentonite sample with active continental margin chemistry (bentonite S_PH0157) is estimated to be 89.4 $^{+0.9}/_{-1.0}$ Ma (95 % credible interval; Fig. 9). Computing similar interpolation models for the sections at Glacier Fiord and the Hoodoo Dome using the U–Pb zircon CA-ID-TIMS ages from Davis *et al.* (2016) permits chronostratigraphic correlation across the basin (Fig. 10). Figures illustrating these interpolation models are available in the online Supplementary Material.

The new U–Pb zircon ages bracket the intervening portion of the Kanguk Formation in section ES2 to the upper Turonian to
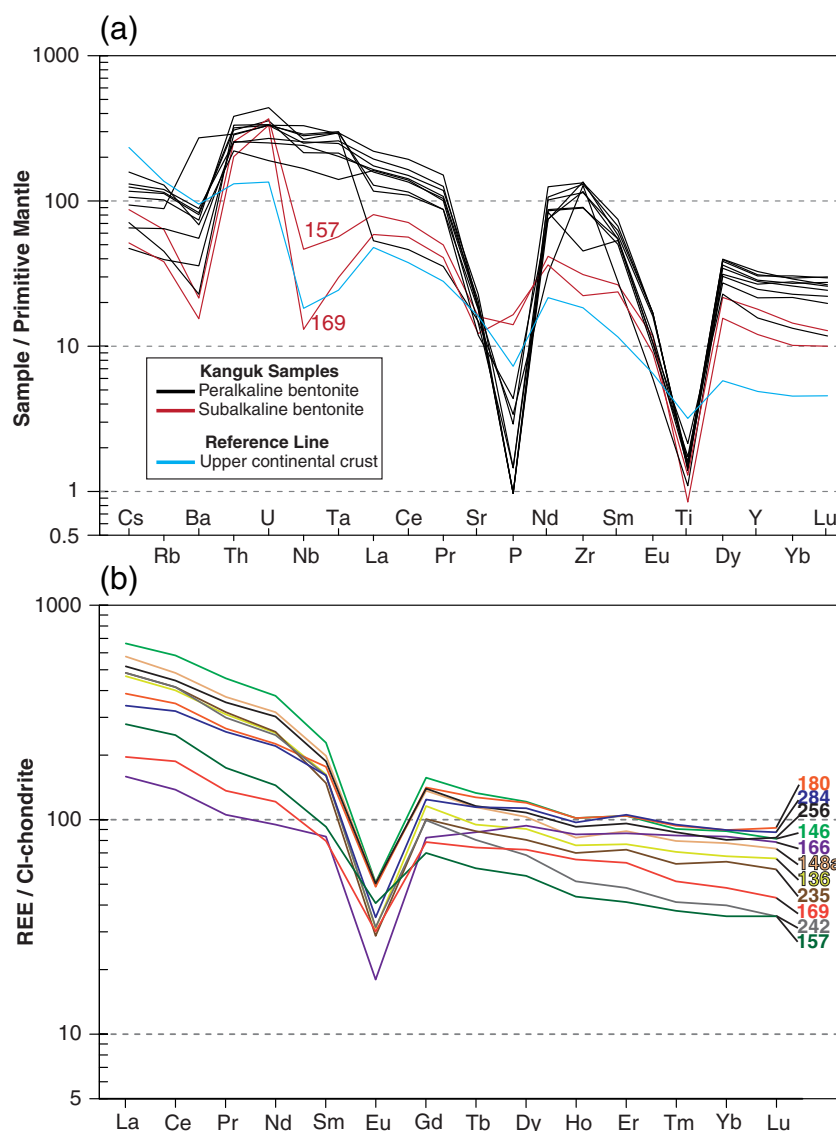
Fig. 7. (Colour online) (a) Primitive-mantle normalized multi-element diagram (normalized to the values of McDonough & Sun, 1995). The reference line for the upper continental crust is drawn according to Rudnick & Gao (2003). (b) Whole-rock rare earth element data from the Kanguk Formation bentonites normalized to the CI-chondrite values of McDonough & Sun (1995).

lower Campanian interval (Fig. 9). Furthermore, these data suggest that the Cenomanian to lower Turonian interval, including an expression of OAE2, is either missing or highly condensed in this section.

The positions of chronostratigraphic boundaries within section ES2 were inferred previously by Davies *et al.* (2018; Fig. 9) using benthic Foraminifera biostratigraphy and by matching of $\delta^{13}C$ isotope data to composite curves from the Western Interior Basin of North America (Joo & Sageman, 2014) and England (Jarvis *et al.* 2006). In comparing our interpolated stage boundaries, there is reasonable agreement for the position of the basal Coniacian Stage boundary but poorer agreement for the basal Santonian and Campanian Stage boundaries (Fig. 9). Davies *et al.* (2018) equated the base of the Coniacian Stage with the same level as bentonite S_PH0146 (Fig. 9); however, the U–Pb date from this bentonite of 91.3 $^{+0.5}/_{-1.0}$ Ma (96.9 % confidence; Table 1) constrains the boundary to be above this level. Our U–Pb interpolation model places the basal Coniacian boundary 7–8 m above this bentonite (Fig. 9). The base Santonian boundary is poorly constrained

in our interpolation model owing to a lack of bentonite age control from near to this stratigraphic level (Fig. 9). The position of the base Campanian boundary is also imprecisely constrained, although it is positioned at a higher level within the section compared to Davies *et al.* (2018), who placed the boundary below a short $\delta^{13}C$ isotope excursion inferred to represent a Santonian–Campanian boundary event (Fig. 9). This isotope excursion occurs within a brown mudstone/shale unit containing numerous siderite(?) nodules and beds (Fig. 9). Furthermore, no correlative of this isotopic event was identified in a nearby section at Slidre Fiord, Ellesmere Island, by Davies *et al.* (2018). Consequently, this excursion may be lithologically controlled and of only local significance. The base of the Campanian Stage in our interpolation model is located close to the first occurrence of the inoceramid bivalve *Sphenoceramus patootensis*, a latest Santonian to early Campanian boreal marker species (Fig. 9). *S. patootensis* forms part of a late Santonian to early Campanian *Sphenoceramus* association that has been reported from the upper Kanguk Formation across the entire Sverdrup Basin, where it occurs in a single or several closely

Table 1. U–Pb zircon SIMS TuffZirc dates obtained from the Kanguk Formation bentonites

| Bentonite	Age (Ma)	Age uncertainty (Ma) +	Age uncertainty (Ma) −	Confidence level	n
S_PH0256	83.1	1.0	2.1	93.5	11/14
S_PH0169	88.5	0.4	1.5	96.1	12/17
S_PH0146	91.3	0.5	1.0	96.9	18/23
S_PH0136	90.4	1.0	0.8	97.8	13/15

n – number of analyses included in age calculation / total number of analyses.

spaced horizons (e.g. Tozer & Thorsteinsson, 1964; Pugh *et al.* 2014; Schröder-Adams *et al.* 2014; Davies *et al.* 2018). Revising the position of the basal Campanian boundary to a higher level within the Sawtooth Range section removes the diachroneity between the first appearance datum of the foraminifer *Glaphyrammina spirocompressa* and the bivalve *Sphenoceramus patootensis* in this section compared to other sites within the Sverdrup Basin (Fig. 10).

5.b. Original ash composition and tectonic setting of source volcanoes

A peralkaline rhyolitic to trachytic ash composition is inferred for all bentonites except S_PH0157 and S_PH0169 using the Zr/TiO_2 versus Nb/Y classification diagram (Fig. 8a). An evolved (felsic) magmatic source is further supported by the presence of sizeable negative europium anomalies in these samples (Fig. 7b). In other studies of bentonites, these anomalies have been inferred to arise through the removal of plagioclase feldspar during fractional crystallization and to indicate an evolved (felsic) magmatic parentage (e.g. Bohor & Triplehorn, 1993; Wray, 1995; Huff *et al.* 1996). The high zirconium concentrations (475–1420 ppm) coupled with a poor recovery of zircon are consistent with a peralkaline composition, as laboratory experiments have demonstrated that zircon solubility increases dramatically as a function of peralkalinity $((Na_2O + K_2O)/Al_2O_3$; Watson, 1979; Linnen & Keppler, 2002). A peralkaline rhyolitic to trachytic ash composition is consistent with previous work by Parsons (1994; Fig. 8). Additional support for such an ash composition is obtained by comparing the data from these Kanguk Formation bentonites with equivalent geochemistry data from Permian tonsteins (kaolinitic, diagenetically altered, volcanic ash layers) in the Songzao Coalfield, China (Dai *et al.* 2011; Table 2). Dai *et al.* (2011) characterized three types of tonstein (mafic, silicic and alkali) that were differentiated using TiO_2/Al_2O_3 ratios and a suite of trace and REEs. In brief, alkali tonsteins show significant enrichment in Nb, Ta, Zr, Hf, REEs and Ga, whilst silicic tonsteins have low REE concentrations but exhibit the greatest fractionation between LREEs and HREEs (Table 2). Using the same geochemical indices, these Kanguk Formation bentonites yield value ranges that are substantially different from the silicic tonsteins and partially overlap with the alkali tonsteins (Table 2). This is except for TiO_2/Al_2O_3 values, which fall between those of silicic and alkali tonsteins.

Using the tectonic discrimination diagrams of Schandl & Gorton (2002), these peralkaline bentonites plot as a tight cluster in the within-plate volcanic zones field (Fig. 8b, c). Such a tectonic setting is consistent with the inferred peralkaline
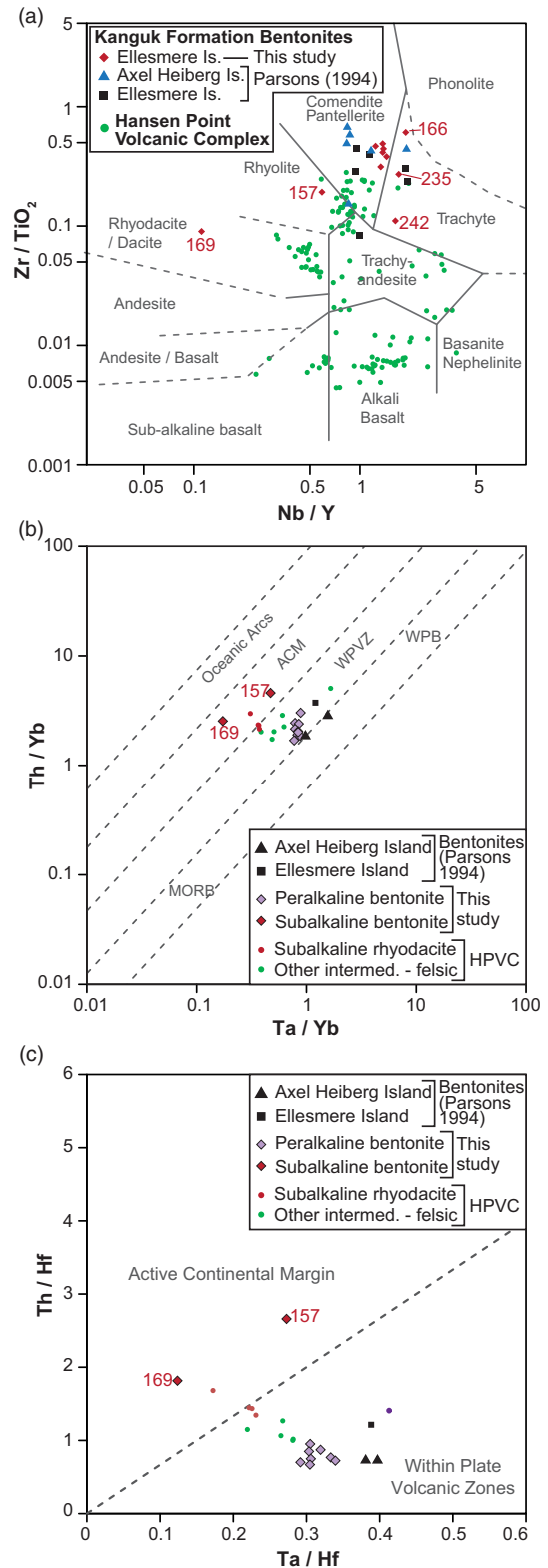
Fig. 8. (Colour online) Trace-element classification and tectonic discrimination diagrams. (a) is after Winchester & Floyd (1977). Is. – island. (b, c) are after Schandl & Gorton (2002). ACM – active continental margins; MORB – mid-ocean ridge basalts; WPB – within-plate basalts; WPVZ – within-plate volcanic zones. Kanguk Formation bentonite whole-rock geochemistry data from Parsons (1994) are also drawn. Whole-rock geochemistry data from the Hansen Point Volcanic Complex (HPVC) are redrawn from Trettin (1996), Estrada & Henjes-Kunst (2004) and Estrada *et al.* (2016).
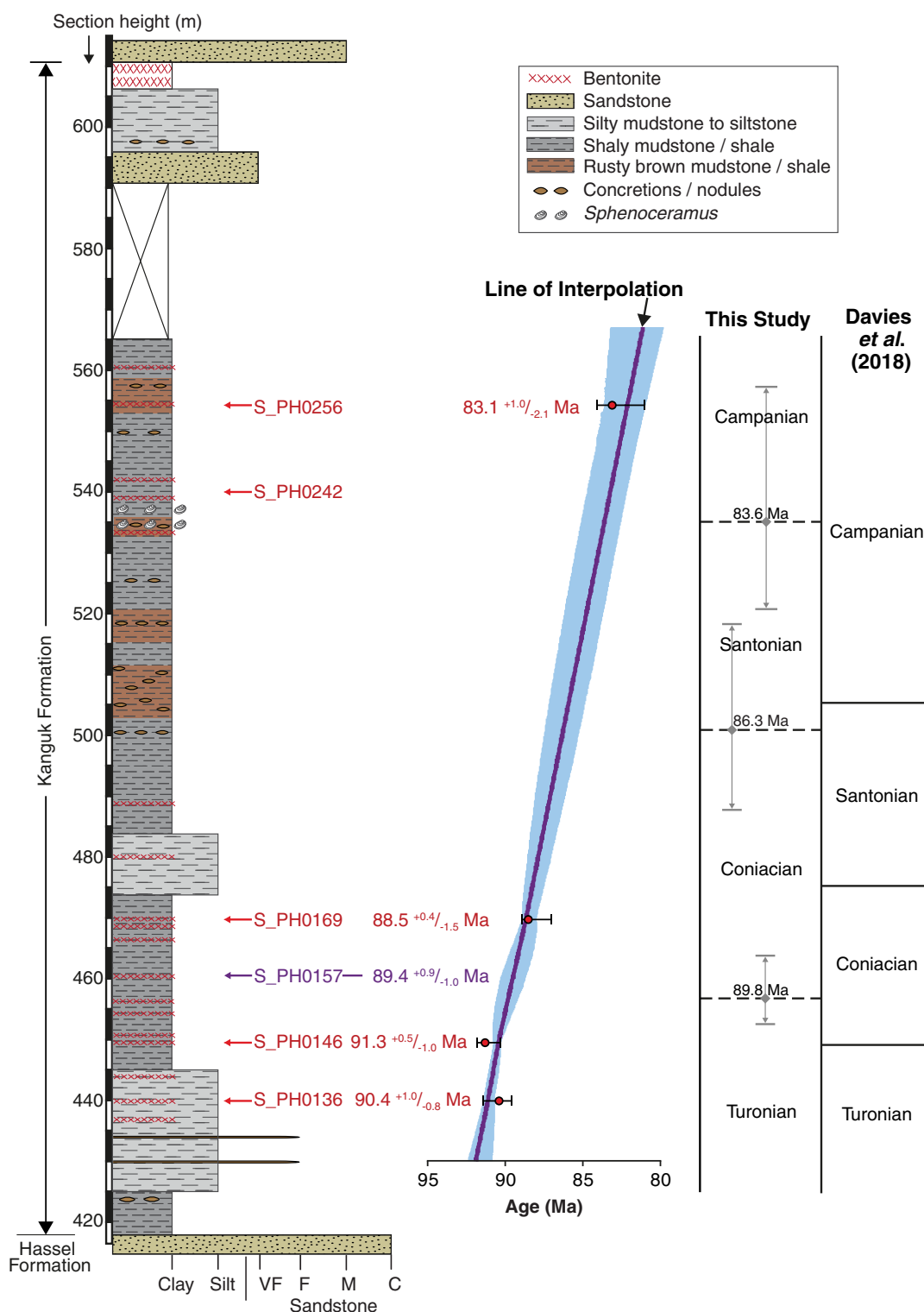
Fig. 9. (Colour online) Age versus stratigraphic height interpolation model for section ES2 calculated using the U–Pb zircon SIMS dates. Interpolation between bentonite horizons was done using the P_Sequence routine of the OXCAL program (Bronk Ramsey, 2008; Bronk Ramsey & Lee, 2013). The pale grey (blue online) band surrounding the line of interpolation denotes the 95 % credible interval of the interpolation model. Numerical ages for the stage boundaries are from Cohen *et al.* (2013). Uncertainties in the positions of stage boundaries are represented by grey vertical lines. The positions of stage boundaries inferred by Davies *et al.* (2018) using a combination of benthic Foraminifera biostratigraphy and δ13C chemostratigraphy are also shown. Note that the age of bentonite S_PH0157 is estimated from the interpolation model.

rhyolitic/trachytic ash composition, as the majority of peralkaline felsic rocks exposed globally are associated with continental extensional (rift) settings (MacDonald, 1974). The conspicuous lack of negative Nb–Ta anomalies in these bentonites further

supports an intraplate tectonic setting with minimal crustal contamination.

Bentonites S_PH0157 and S_PH0169 show geochemical differences to the other bentonites analysed. They plot within the
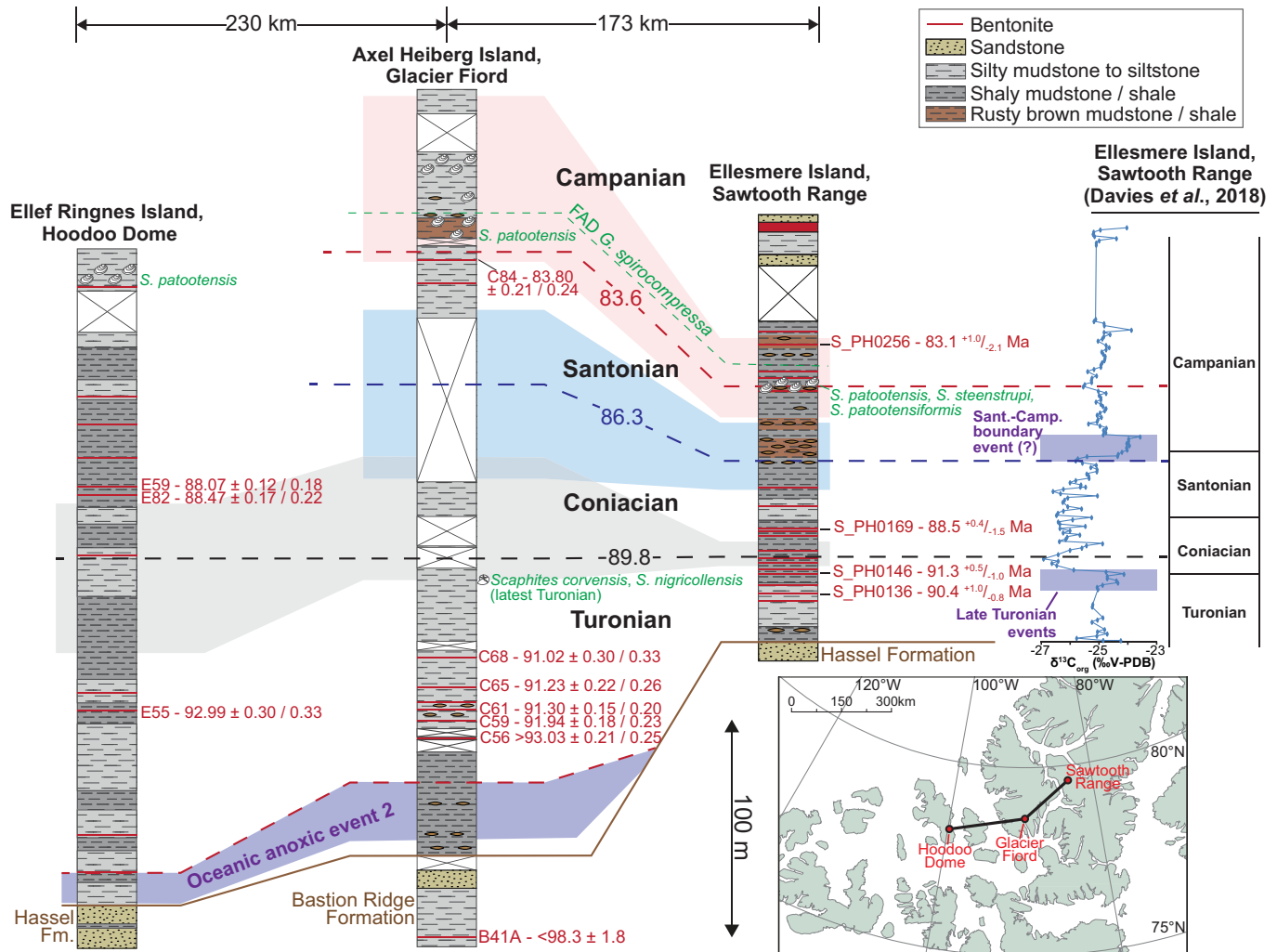
Fig. 10. (Colour online) Correlation panel for the Kanguk Formation based on U–Pb ages from interbedded bentonites. For each section, an age versus height interpolation model was calculated using OXCAL (Bronk Ramsey, 2008; Bronk Ramsey & Lee, 2013); chronostratigraphic stage boundaries, represented by dashed lines, were correlated between sections from these. The uncertainty in positions of chronostratigraphic boundaries is denoted by the shaded (colour online) bands surrounding the boundaries. These represent the 95 % credible interval of the interpolation models. The Glacier Fiord and Hoodoo Dome sections are redrawn and simplified from Schröder-Adams *et al.* (2014) and Pugh *et al.* (2014), respectively. CA-ID-TIMS dates from these two sections are from Davis *et al.* (2016). ± X/Y uncertainty levels (*sensu* Schoene *et al.* 2006) are shown for the CA-ID-TIMS data; X uncertainties are relevant for the comparison of the CA-ID-TIMS dates, whereas the Y uncertainties are relevant when comparing the CA-ID-TIMS dates to our SIMS dates. First appearance datums (FAD) for *G. spirocompressa* are from Schröder-Adams *et al.* (2014) and Davies *et al.* (2018). δ¹³C_org data are redrawn from Davies *et al.* (2018); horizontal shaded bars denote intervals containing positive isotope excursions identified by the authors.

subalkaline rhyolite and dacite/rhyodacite fields in the Zr/TiO_2 versus Nb/Y classification diagram (Fig. 8a). Furthermore, these bentonites have negative Nb–Ta anomalies (Fig. 7a), smaller negative europium anomalies (Fig. 7b) and the lowest concentrations of zirconium and REEs apart from bentonite S_PH0166. Taken together these data indicate a different, subalkaline dacitic to rhyolitic ash composition for these two bentonites. Bentonites S_PH0157 and S_PH0169 plot in the active continental margin field in Figure 8b, c. Such a tectonic setting is consistent with the negative Nb–Ta anomalies present in these bentonites, which are a prominent geochemical feature of subduction zone magmatism (Baier *et al.* 2008). Negative Nb–Ta anomalies are, however, not unique to active continental margins and can occur in magmatic rocks from other tectonic settings; for example, magma generated in an anorogenic continental setting can gain arc-like geochemical characteristics through extensive crustal assimilation (e.g. Pearce, 2014).

Taken together, the available data support that there are two distinct types of bentonite within the Kanguk Formation which

were likely sourced from volcanic centres within different tectonic regimes. These are as follows: (1) thick (mostly 20–80 cm), *c.* 92–83 Ma peralkaline rhyolitic to trachytic ashes with geochemistry suggestive of an intraplate tectonic setting (n = 9); (2) thin (<5 cm), *c.* 90–88 Ma subalkaline dacitic to rhyolitic ashes likely originating from an active continental margin setting (bentonites S_PH0157 and S_PH0169).

5.c. Possible locations of the source volcanoes

5.c.1. Peralkaline bentonites

The volcanic source(s) of intraplate, peralkaline bentonites within the Kanguk Formation has been discussed in other studies (Parsons, 1994; Davis *et al.* 2016) that concluded they were locally sourced from igneous centres on the Sverdrup Rim, Alpha Ridge, northern Ellesmere Island and/or northern Greenland. Davis *et al.* (2016) inferred ash transportation distances of <1000 km for these bentonites on the basis of 10–40 cm bed thicknesses.

Table 2. Comparison of whole-rock geochemistry data from bentonites of the Kanguk Formation to Permian mafic, silicic and alkali tonsteins of the Songzao Coalfield, China (Dai *et al.* 2011). Data are expressed as minimum and maximum ranges

	Songzao Coalfield tonsteins			Kanguk Formation bentonites	
	Mafic	Alkali	Silicic	Peralkaline	Subalkaline
Ti/Al_2O_3	0.087 – 0.119	0.037 – 0.079	0.008 – 0.02	0.024 – 0.032	0.010 – 0.015
Ga/Al_2O_3	1.02 – 2.83	1.5 – 2.22	0.57 – 1.1	2.3 – 4.1	1.4 – 1.6
Zr/Al_2O_3	20.7 – 126.2	15.5 - 357	2.2 – 6.5	35.6 – 157.1	13.6 – 19.6
Hf/Al_2O_3	0.74 – 4.6	0.36 – 4.8	0.09 – 0.2	0.94 – 3.69	0.46 – 0.52
Nb/Al_2O_3	8.8 – 16.7	1.6 – 6.3	0.2 – 0.5	8.2 – 25.4	0.5 – 1.8
Ta/Al_2O_3	0.3 – 1.4	0.11 – 0.39	0.06 – 0.1	0.39 – 1.25	0.06 – 0.13
ΣREE	190 – 5860	44 – 1503	145 – 388	244.9 – 790.0	248.3 – 284.5
La_N/Yb_N*	2.2 – 21	3.2 – 14.9	18.1 – 46.4	1.9 – 12.2	4.1 – 7.9
Number†	17	13	5	9	2

*Calculated using data normalized to CI-chondrite values (McDonough & Sun, 1995).
†Number of analyses used to calculate the data ranges.

Peralkaline bentonites in section ES2 are ~10–500 cm thick (Fig. 3), which, together with the coarse size of zircon phenocrysts in the Turonian bentonites S_PH0136 and S_PH0146, corroborates that the source volcanoes were proximal to the Sverdrup Basin.

Within this geographical radius there are known alkaline mafic to felsic volcanic and intrusive rocks exposed locally on northern Ellesmere Island that have compatible geochemistry and overlapping age (Fig. 11). Local 92–90 Ma bimodal alkaline igneous rocks of the Wootton Intrusive Complex are exposed to the north of the Sverdrup Basin, on northern Ellesmere Island (Trettin & Parrish, 1987; Estrada & Henjes-Kunst, 2013). The complex comprises predominantly gabbro, with minor granitoids and hybrid rocks (Trettin & Parrish, 1987; Estrada *et al.* 2006), although 93–91 Ma hypabyssal alkali-feldspar- and quartz-bearing microgranites with peralkaline rhyolitic chemistry have also been reported (Estrada *et al.* 2006; Estrada & Henjes-Kunst, 2013).

Similarly, the Hansen Point volcanic complex (HPVC) exposed on northern Ellesmere Island is characterized by transitional to mildly alkaline, mafic to felsic volcanic rocks (Trettin & Parrish, 1987; Embry & Osadetz, 1988; Embry, 1991; Trettin, 1996; Estrada & Henjes-Kunst, 2004; Estrada *et al.* 2006), except for voluminous subalkaline rhyodacites and the dolerites within the vicinity of Yelverton Bay (Fig. 1). HPVC volcanic rocks largely have an intraplate geochemical affinity (Fig. 8b, c), and were likely erupted in a continental rift setting (Estrada & Henjes-Kunst, 2004, 2013). This is apart from the subalkaline rhyodacites that show more transitional geochemistry and plot close to or within the active continental margin field in Figure 8b, c. Their transitional chemistry has been attributed to crustal contamination of the parent magma (Estrada *et al.* 2016). The majority of these volcanic rocks are interpreted to have been erupted subaerially, although some interbedded shales contain dinoflagellates, indicating a marine environment (Embry & Osadetz, 1988). These shales have yielded very similar dinoflagellate assemblages to those of the Kanguk Formation (Embry, 1991), suggesting the two may in part be coeval. Several Ar–Ar and Rb–Sr dates have been published, which yield a wide range of ages from 45–95 Ma, although most are within the 75–95 Ma age range (Estrada & Henjes-Kunst, 2004; Bono *et al.* 2013; Estrada & Henjes-Kunst, 2013). Few U–

Pb dates exist from the HPVC; a U–Pb TIMS age from a porphyritic rhyodacite (88 $^{+20}/_{-21}$ Ma; Trettin & Parrish, 1987) is too imprecise to provide meaningful comparison with the U–Pb bentonite dates from the Kanguk Formation. Three recent U–Pb LA-ICP-MS dates of 104–96 Ma from subalkaline rhyodacites to the west of Yelverton Bay (Estrada *et al.* 2016) pre-date the deposition of the Kanguk Formation bentonites. Based on still sparse age data, HPVC magmatism, at least within the Yelverton Bay area, lasted from *c.* 122 to 74 Ma and changed from a subalkaline to dominantly mildly alkaline character since *c.* 96 Ma (Estrada *et al.* 2016).

On the basis of available age data, a Greenland source for the peralkaline Kanguk bentonites is unlikely. The bimodal Kap Washington Group exposed on North Greenland contains units with similar chemistry to the peralkaline Kanguk Formation bentonites (trachytic to rhyolitic lavas and ignimbrites, and fewer mildly alkaline basalts; Thórarinsson *et al.* 2011). Available isotopic ages, however, suggest that the felsic portions of the group were erupted after 71 Ma (Tegner *et al.* 2011; Thórarinsson *et al.* 2011) and thus after the Kanguk Formation bentonites. Older (85–80 Ma) alkaline dykes are known from North Greenland, but these are of mafic composition (Kontak *et al.* 2001; Thórarinsson *et al.* 2015).

5.c.2. Subalkaline bentonites

On the basis of available age and geochemistry data from the HPVC, this volcanic complex is an unlikely source area for the two *c.* 90–88 Ma bentonites with subalkaline geochemistry. This is because the complex at this time is thought to have been characterized by mildly alkaline, intraplate magmatism (Estrada *et al.* 2016; see Section 5.c.1). The two bentonites with subalkaline geochemistry are notably thinner than the peralkaline bentonites and contain small zircon grains (typically 50–80 μm in length). Thus, it is possible that these bentonites originated from further afield compared to those with peralkaline chemistry. The subalkaline bentonites have geochemical characteristics that are consistent with an active continental margin tectonic setting (Section 5.b). The closest destructive plate margin at this time was ~3000 km away, along the western margin of North America and the eastern margin of Russia (Fig. 11).
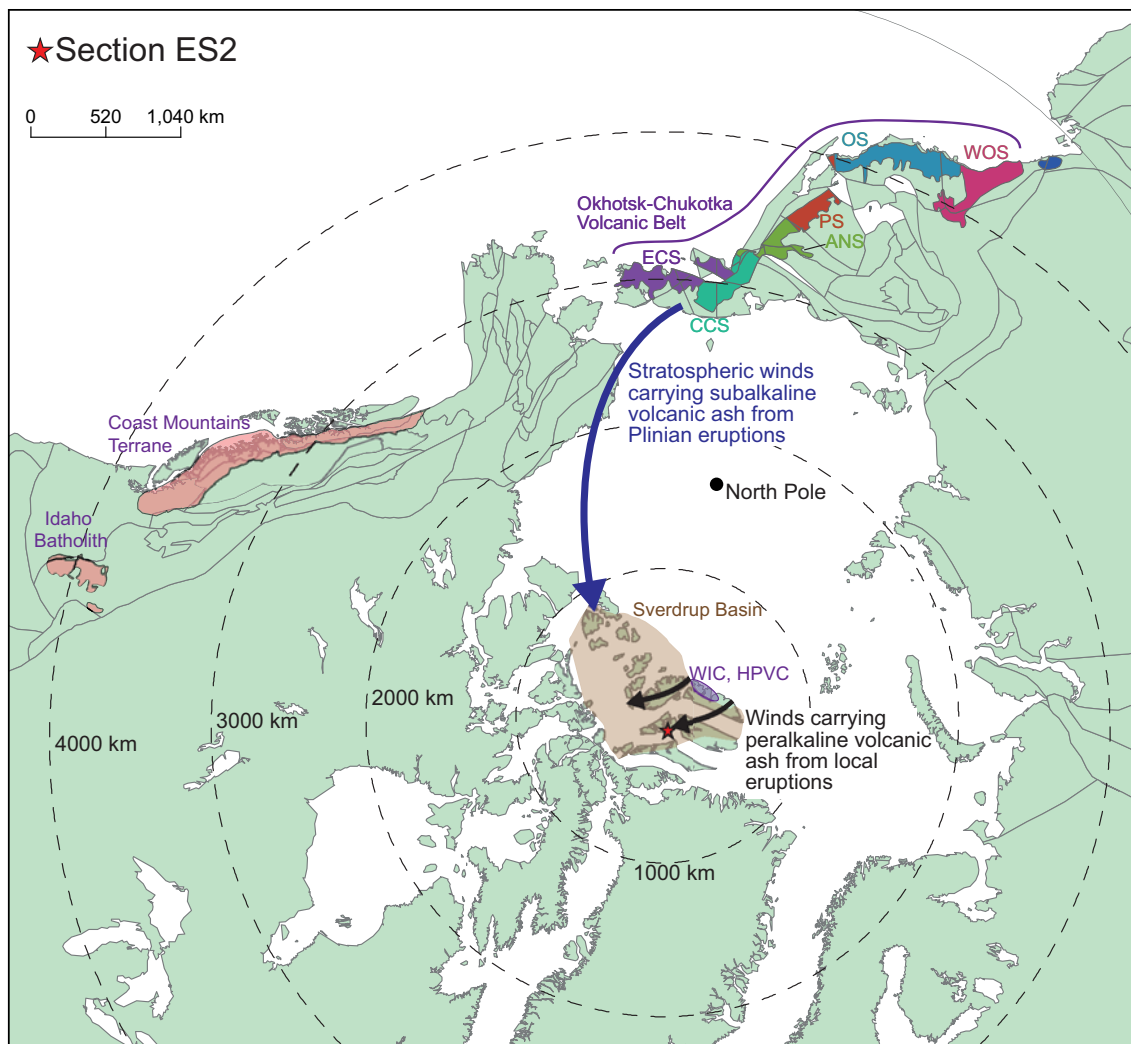
Fig. 11. (Colour online) Plate tectonic reconstruction of the circum-Arctic region during Late Cretaceous times (89 Ma) created in GPlates (v. 2) using the model of Matthews *et al.* (2016). The Coast Mountains Terrane is redrawn from Wheeler *et al.* (1991); the Coast Mountains Batholith comprises the majority of the Coast Mountains Terrane. The Okhotsk–Chukotka Volcanic Belt is redrawn from Tikhomirov *et al.* (2012). The Hanson Point Volcanic Complex (HPVC) and Wootton Intrusive Complex (WIC) are simplified from Estrada *et al.* (2016). Abbreviations for segments within the Okhotsk–Chukotka Volcanic Belt (from Tikhomirov *et al.* 2012): ANS – Anadyr segment; CCS – Central Chukotka segment; ECS – East Chukotka segment; OS – Okhotsk segment; PS – Penzhina segment; WOS – West Okhotsk segment.

There is evidence of considerable Late Cretaceous magmatism along the West Coast of North America. This is exemplified by the Coast Mountains and Idaho batholiths (Fig. 11; Gehrels *et al.* 2009; Gaschnig *et al.* 2010; Cecil *et al.* 2011). However, only local evidence remains of any associated volcanism, following subsequent uplift and erosion (Miller *et al.* 2002). In contrast, there is a substantial volume of subalkaline felsic volcanic rocks preserved within the Okhotsk–Chukotka Volcanic Belt (OCVB; Tikhomirov *et al.* 2008, 2012; Akinin & Miller, 2011; Pease *et al.* 2018). Using U–Pb and Ar–Ar age data, Tikhomirov *et al.* (2012) identified several episodes of peak volcanism within the northern part of the volcanic belt, which occurred during *c.* 82–79, 85.5–84 and 89–87 Ma. Based on the available geochemical and U–Pb age data, bentonites S_PH0157 and S_PH0169 are compatible with a volcanic source in the northern OCVB. Volcanism in the OCVB is thought to have been most intense during *c.* 89–84 Ma, with considerable thicknesses (1–2 km) of predominantly felsic volcanic rocks accumulated over a large area of the central Chukchi segment (Akinin & Miller, 2011; Tikhomirov *et al.* 2012). This has been interpreted to represent catastrophic Plinian-type volcanism that was comparable

in volume, duration and composition to that of a silicic large igneous province (Tikhomirov *et al.* 2012).

A lack of ash deposits to the west of the OCVB has been interpreted as evidence of predominant Late Cretaceous winds from NE Russia towards Alaska (Spicer & Herman, 2010), and by extension, the Sverdrup Basin. Numerous bentonites have been reported from Upper Cretaceous strata on the North Slope of Alaska (Seabee, Schrader Bluff, Prince Creek formations and the Hue Shale; e.g. Molenaar *et al.* 1987; Mull *et al.* 2003) and the Mackenzie Delta area, Canada (Boundary Creek and Smoking Hills sequences; Dixon, 1996, pp. 73–4), which have been suggested to have originated from the OCVB (e.g. Miller *et al.* 2002; Bergman *et al.* 2006; Houseknecht & Bird, 2011). Large volcanic eruptions, of Plinian to ultra-Plinian scale, injecting volcanic ash high into the stratosphere would have been required to facilitate volcanic ash transportation over such great distances. It is feasible, that during 89–84 Ma, intense volcanism within the OCVB resulted in substantial volcanic ash being injected into the stratosphere, leading to widespread volcanic ash dispersal across Arctic Alaska and Canada, reaching as far east as the Sverdrup Basin (Fig. 11).

6. Conclusions

Two distinct types of bentonite are identified within the Kanguk Formation on the basis of whole-rock geochemical analyses from an outcrop section in the Sawtooth Range, Ellesmere Island. Numerous relatively thick (~10–500 cm) peralkaline rhyolitic to trachytic bentonites possessing geochemical affinities consistent with an intraplate tectonic setting occur at several levels within an upper Turonian to lower Campanian outcrop section. These are likely the products of local volcanism associated with the alkaline phase of the HALIP. Thinner (<5 cm) subalkaline dacitic to rhyolitic bentonites are consistent with an active continental margin setting. From the available data, these appear to be confined to the upper Turonian to lower Coniacian. The lack of nearby potential sources of subalkaline magmatism, together with the thinner bed thickness of the subalkaline bentonites, supports a more distal source area. The age and geochemistry of the subalkaline bentonites correlate with an interval of intense volcanism in the OCVB, Russia. Numerous bentonites have been reported from Upper Cretaceous strata on the North Slope of Alaska and in the Mackenzie Delta area, which have been suggested to have originated from the OCVB by other workers (e.g. Miller *et al.* 2002; Bergman *et al.* 2006; Houseknecht & Bird, 2011). It is proposed that during early Coniacian times intense volcanism within this volcanic belt resulted in widespread volcanic ash dispersal across Arctic Alaska and Canada, reaching as far east as the Sverdrup Basin.

Author ORCIDs. Michael A Pointon, 0000-0003-1992-0053; Michael J Flowerdew, 0000-0002-9710-2593; Peter Hülse, 0000-0002-0264-7583; Simon Schneider, 0000-0001-6493-357X; Martin J Whitehouse, 0000-0003-2227-577X

References

Akinin VV and Miller EL (2011) Evolution of calc-alkaline magmas of the Okhotsk-Chukotka volcanic belt. *Petrology* **19**, 237–77.

Baier J, Audétat A and Keppler H (2008) The origin of the negative niobium tantalum anomaly in subduction zone magmas. *Earth and Planetary Science Letters* **267**, 290–300.

Balkwill H and Hopkins W (1976) Cretaceous stratigraphy, Hoodoo Dome, Ellef Ringnes Island, District of Franklin. *Geological Survey of Canada, Paper 76*, 329–34.

Bea F (1996) Residence of REE, Y, Th and U in granites and crustal protoliths; implications for the chemistry of crustal melts. *Journal of Petrology* **37**, 521–52.

Bergman SC, Akinin VV, Decker J, Miller EL and Layer P (2006) North Alaska Upper Cretaceous tephra: Eurasian or North American source calderas? In *102nd Annual Meeting of the Cordilleran Section, GSA, 81st Annual Meeting of the Pacific Section, AAPG, and the Western Regional Meeting of the Alaska Section, SPE, 8–10 May 2006, Anchorage, Alaska. Geological Society of America Abstracts with Programs* 38, 90.

Black LP, Kamo SL, Allen CM, Davis DW, Aleinikoff JN, Valley JW, Mundil R, Campbell IH, Korsch RJ, Williams IS and Foudoulis C (2004) Improved $^{206}Pb/^{238}U$ microprobe geochronology by the monitoring of a trace-element-related matrix effect; SHRIMP, ID–TIMS, ELA–ICP–MS

and oxygen isotope documentation for a series of zircon standards. *Chemical Geology* **205**, 115–40.

Bohor BF and Triplehorn DM (1993) *Tonsteins: Altered Volcanic Ash Layers in Coal-Bearing Sequences*. Geological Society of America, Special Paper 285, 44 pp.

Bono R, Tarduno J and Singer B (2013) Cretaceous magmatism in the High Canadian Arctic: implications for the nature and age of Alpha Ridge. In *EGU General Assembly Conference, 7–12 April 2013, Vienna, Austria, Abstracts no. 11429*.

Bono RK, Clarke J, Tarduno JA and Brinkman D (2016) A large ornithurine bird (*Tingmiatornis arctica*) from the Turonian High Arctic: climatic and evolutionary implications. *Scientific Reports* **6**, 38876. doi: 10.1038/srep38876.

Bronk Ramsey C (2008) Deposition models for chronological records. *Quaternary Science Reviews* **27**, 42–60.

Bronk Ramsey C and Lee S (2013) Recent and planned developments of the program OxCal. *Radiocarbon* **55**, 720–30.

Cecil MR, Gehrels G, Ducea MN and Patchett PJ (2011) U–Pb–Hf characterization of the central Coast Mountains batholith: implications for petrogenesis and crustal architecture. *Lithosphere* **3**, 247–60.

Christidis GE (1998) Comparative study of the mobility of major and trace elements during alteration of an andesite and a rhyolite to bentonite, in the islands of Milos and Kimolos, Aegean, Greece. *Clays and Clay Minerals* **46**, 379–99.

Christidis GE, Scott PS and Marcopoulos T (1995) Origin of the bentonite deposits of eastern Milos, Aegean, Greece; geological, mineralogical and geochemical evidence. *Clays and Clay Minerals* **43**, 63–77.

Claiborne LL, Miller CF and Wooden JL (2010) Trace element composition of igneous zircon: a thermal and compositional record of the accumulation and evolution of a large silicic batholith, Spirit Mountain, Nevada. *Contributions to Mineralogy and Petrology* **160**, 511–31.

Cohen, KM, Finney, SC, Gibbard, PL and Fan, J-X (2013) The ICS international chronostratigraphic chart. *Episodes* **36**, 199–204.

Dai S, Wang X, Zhou Y, Hower JC, Li D, Chen W, Zhu X and Zou J (2011) Chemical and mineralogical compositions of silicic, mafic, and alkali tonsteins in the late Permian coals from the Songzao Coalfield, Chongqing, Southwest China. *Chemical Geology* **282**, 29–44.

Davies MA, Schröder-Adams CJ, Herrle JO, Hülse P, Schneider S, Quesnel A and Harwood DM (2018) Integrated biostratigraphy and carbon isotope stratigraphy for the Upper Cretaceous Kanguk Formation of the High Arctic Sverdrup Basin, Canada. *Geological Society of America Bulletin* **130**, 1540–61.

Davis WJ, Schröder-Adams CJ, Galloway JM, Herrle JO and Pugh AT (2016) U–Pb geochronology of bentonites from the Upper Cretaceous Kanguk Formation, Sverdrup Basin, Arctic Canada: constraints on sedimentation rates, biostratigraphic correlations and the late magmatic history of the High Arctic Large Igneous Province. *Geological Magazine* **154**, 757–76.

Dixon J (1996) *Geological Atlas of the Beaufort-Mackenzie Area*. Geological Survey of Canada, Miscellaneous Report 59, 173 pp.

Dostal J and MacRae A (2018) Cretaceous basalts of the High Arctic large igneous province at Axel Heiberg Island (Canada): volcanic stratigraphy, geodynamic setting, and origin. *Geological Journal* **53**, 2918–34.

Embry AF (1991) Mesozoic history of the Arctic islands. In *Geology of the Innuitian Orogen and Arctic Platform of Canada and Greenland* (ed HP Trettin), pp. 371–430. Geology of Canada Series no. 3. Ottawa: Geological Survey of Canada.

Embry AF and Beauchamp B (2008) Sverdrup Basin. In *The Sedimentary Basins of the United States and Canada, vol. 5* (ed AD Miall), pp. 451–71. Amsterdam: Elsevier.

Embry AF and Dixon J (1990) The breakup unconformity of the Amerasia Basin, Arctic Ocean: evidence from Arctic Canada. *Geological Society of America Bulletin* **102**, 1526–34.

Embry AF and Osadetz KG (1988) Stratigraphy and tectonic significance of Cretaceous volcanism in the Queen Elizabeth Islands, Canadian Arctic Archipelago. *Canadian Journal of Earth Sciences* **25**, 1209–19.

Estrada S, Damaske D, Henjes-Kunst F, Schreckenberger B, Oakey GN, Piepjohn K, Eckelmann K and Linnemann U (2016) Multistage Cretaceous magmatism in the northern coastal region of Ellesmere Island and its relation to the formation of Alpha Ridge–evidence from

aeromagnetic, geochemical and geochronological data. *Norwegian Journal of Geology* **96**, 65–95.

Estrada S and Henjes-Kunst F (2004) Volcanism in the Canadian High Arctic related to the opening of the Arctic Ocean. *Zeitschrift der Deutschen Geologischen Gesellschaft* **154**, 579–603.

Estrada S and Henjes-Kunst F (2013) ⁴⁰Ar–³⁹Ar and U–Pb dating of Cretaceous continental rift-related magmatism on the northeast Canadian Arctic margin. *Zeitschrift der Deutschen Gesellschaft für Geowissenschaften* **164**, 107–30.

Estrada S, Piepjohn K, Henjes-Kunst F and von Gosen W (2006) Geology, magmatism and structural evolution of the Yelverton Bay area, northern Ellesmere Island, Arctic Canada. *Polarforschung* **73**, 59–75.

Floyd PA and Winchester JA (1978) Identification and discrimination of altered and metamorphosed volcanic rocks using immobile elements. *Chemical Geology* **21**, 291–306.

Fricker PE (1963) *Geology of the Expedition Area, Western Central Axel Heiberg, Canadian Arctic Archipelago*. Montreal: McGill University, 156 pp.

Gaschnig RM, Vervoort JD, Lewis RS and McClelland WC (2010) Migrating magmatism in the northern US Cordillera: in situ U–Pb geochronology of the Idaho batholith. *Contributions to Mineralogy and Petrology* **159**, 863–83.

Gehrels G, Rusmore M, Woodsworth G, Crawford M, Andronicos C, Hollister L, Patchett J, Ducea M, Butler R, Klepeis K, Davidson C, Friedman R, Haggart J, Mahoney B, Crawford W, Pearson D and Girardi J (2009) U–Th–Pb geochronology of the Coast Mountains batholith in north-coastal British Columbia: constraints on age and tectonic evolution. *Geological Society of America Bulletin* **121**, 1341–61.

Hadlari, T, Midwinter, D, Galloway, JM, Dewing, K and Durbano, AM (2016) Mesozoic rift to post-rift tectonostratigraphy of the Sverdrup Basin, Canadian Arctic. *Marine and Petroleum Geology* **76**, 148–58.

Harrison JC, St-Onge MR, Petrov OV, Strelnikov SI, Lopatin BG, Wilson FH, Tella S, Paul D, Lynds T, Shokalsky SP, Hults CK, Bergman S, Jepsen HF and Solli A (2011) *Geological Map of the Arctic. 'A' Series Map, 2159A*. Ottawa: Geological Survey of Canada.

Herrle JO, Schröder-Adams CJ, Davis W, Pugh AT, Galloway JM and Fath J (2015) Mid-Cretaceous High Arctic stratigraphy, climate, and Oceanic Anoxic Events. *Geology* **43**, 403–6.

Hill IG, Worden RH and Meighan IG (2000) Yttrium: the immobility-mobility transition during basaltic weathering. *Geology* **28**, 923–6.

Hoskin PWO, Kinny PD, Wyborn D and Chappell BW (2000) Identifying accessory mineral saturation during differentiation in granitoid magmas: an integrated approach. *Journal of Petrology* **41**, 1365–96.

Houseknecht DW and Bird KJ (2011) Geology and petroleum potential of the rifted margins of the Canada Basin. In *Arctic Petroleum Geology* (eds AM Spencer, AF Embry, DL Gautier, AV Stoupakova and K Sørensen), pp. 509–26. Geological Society of London, Memoir no. 35.

Huff WD, Merriman RJ, Morgan DJ and Roberts B (1993) Distribution and tectonic setting of Ordovician K-bentonites in the United Kingdom. *Geological Magazine* **130**, 93–100.

Huff WD, Morgan DJ and Rundle CC (1996) *Silurian K-bentonites of the Welsh Borderlands: Geochemistry, Mineralogy and K-Ar Ages of Illitization*. British Geological Survey Technical Report WG/96/45, 25 pp.

Inanli FÖ, Huff WD and Bergström SM (2009) The lower Silurian (Llandovery) Osmundsberg K-bentonite in Baltoscandia and the British Isles: chemical fingerprinting and regional correlation. *GFF* **131**, 269–79.

Jaffey AH, Flynn KF, Glendenin LE, Bentley WC and Essling AM (1971) Precision measurement of half-lives and specific activities of ²³⁵U and ²³⁸U. *Physical Review C* **4**, 1889–906.

Jarvis IAN, Gale AS, Jenkyns HC and Pearce MA (2006) Secular variation in Late Cretaceous carbon isotopes: a new δ¹³C carbonate reference curve for the Cenomanian–Campanian (99.6–70.6 Ma). *Geological Magazine* **143**, 561–608.

Jeletzky JA (1970) Marine biotic provinces and palaeogeography of western and Arctic Canada: illustrated by a detailed study of ammonites. *Geological Survey of Canada, Paper* **70**, 1–92.

Jeon, H and Whitehouse, MJ (2015) A critical evaluation of U–Pb calibration schemes used in SIMS zircon geochronology. *Geostandards and Geoanalytical Research* **39**, 443–52.

Joo YJ and Sageman BB (2014) Cenomanian to Campanian carbon isotope chemostratigraphy from the Western Interior Basin, USA. *Journal of Sedimentary Research* **84**, 529–42.

Kiipli T, Dahlqvist P, Kallaste T, Kiipli E and Nõlvak J (2015) Upper Katian (Ordovician) bentonites in the East Baltic, Scandinavia and Scotland: geochemical correlation and volcanic source interpretation. *Geological Magazine* **152**, 589–602.

Kiipli T, Einasto R, Kallaste T, Nestor V, Perens H and Siir S (2011) Geochemistry and correlation of volcanic ash beds from the Rootsiküla Stage (Wenlock–Ludlow) in the eastern Baltic. *Estonian Journal of Earth Sciences* **60**, 207–19.

Kiipli T, Hints R, Kallaste T, Verš E and Voolma M (2017) Immobile and mobile elements during the transition of volcanic ash to bentonite – an example from the early Palaeozoic sedimentary section of the Baltic Basin. *Sedimentary Geology* **347**, 148–59.

Kiipli T, Kallaste T, Kiipli E and Radzevičius S (2013) Correlation of Silurian bentonites based on the immobile elements in the East Baltic and Scandinavia. *GFF* **135**, 152–61.

Kingsbury CG, Kamo SL, Ernst RE, Söderlund U and Cousens BL (2018) U–Pb geochronology of the plumbing system associated with the Late Cretaceous Strand Fiord Formation, Axel Heiberg Island, Canada: part of the 130–90 Ma High Arctic large igneous province. *Journal of Geodynamics* **118**, 106–17.

Kontak DJ, Jensen SM, Dostal J, Archibald DA and Kyser TK (2001) Cretaceous mafic dyke swarm, Peary Land, northernmost Greenland: geochronology and petrology. *The Canadian Mineralogist* **39**, 997–1020.

Lenniger M, Nøhr-Hansen H, Hills LV and Bjerrum CJ (2014) Arctic black shale formation during Cretaceous Oceanic Anoxic Event 2. *Geology* **42**, 799–802.

Li C, Arndt NT, Tang Q and Ripley EM (2015) Trace element indiscrimination diagrams. *Lithos* **232**, 76–83.

Linnen RL and Keppler H (2002) Melt composition control of Zr/Hf fractionation in magmatic processes. *Geochimica et Cosmochimica Acta* **66**, 3293–301.

Ludwig KR (2012) *User's Manual for Isoplot 3.75: A Geochronological Toolkit for Microsoft Excel*. Berkeley Geochronology Center, Special Publication no. 5.

MacDonald R (1974) Tectonic settings and magma associations. *Bulletin Volcanologique* **38**, 575–93.

Matthews KJ, Maloney KT, Zahirovic S, Williams SE, Seton M and Müller RD (2016) Global plate boundary evolution and kinematics since the late Paleozoic. *Global and Planetary Change* **146**, 226–50.

McDonough WF and Sun SS (1995) The composition of the Earth. *Chemical Geology* **120**, 223–53.

Miller EL, Gelman M, Parfenov L and Hourigan J (2002) Tectonic setting of Mesozoic magmatism: a comparison between northeastern Russia and the North American Cordillera. In *Tectonic Evolution of the Bering Shelf–Chukchi Sea–Arctic Margin and Adjacent Landmasses* (eds EL Miller, A Grantz and SL Klemperer), pp. 313–32. Geological Society of America, Special Paper 360.

Molenaar C, Bird K and Kirk A (1987) Cretaceous and Tertiary stratigraphy of northeastern Alaska. In *Alaskan North Slope Geology* (eds I Taileur and P Weimer), pp. 513–28. Bakersfield, California: Society of Economic Paleontologists and Mineralogists.

Mull CG, Houseknecht DW and Bird KJ (2003) *Revised Cretaceous and Tertiary Stratigraphic Nomenclature in the Colville Basin, Northern Alaska*. U.S. Geological Survey Professional Paper 1673, 51 pp.

Núñez-Betelu L, MacRae R, Hills L and Muecke G (1994) Uppermost Albian–Campanian palynological biostratigraphy of Axel Heiberg and Ellesmere Islands (Canadian Arctic). In *Proceedings of the 1992 International Conference on Arctic Margins, 2–4 September 1992, Anchorage, Alaska* (eds D Thurston and K Fujita), pp. 135–40.

Nunez-Betelu LK and Hills LV (1994) *Palynological Data from the Uppermost Hassel and Kanguk Formations and the Lowermost Eureka Sound Group (Uppermost Lower Cretaceous–Paleocene), Axel Heiberg and Ellesmere Islands, Canadian Arctic*. Geological Survey of Canada, Open File 2489, 191 pp.

Parsons MB (1994) *Geochemistry and petrogenesis of Late Cretaceous bentonites from the Kanguk Formation, Axel Heiberg and Ellesmere Islands, Canadian*

High Arctic. B.Sc. thesis, Dalhousie University, Nova Scotia, Canada. Published thesis.

Pearce JA (2014) Geochemical Fingerprinting of the Earth's Oldest Rocks. *Geology* **42**, 175–6.

Pease V, Miller E, Wyld SJ, Sokolov S, Akinin V and Wright JE (2018) U–Pb zircon geochronology of Cretaceous arc magmatism in eastern Chukotka, NE Russia, with implications for Pacific plate subduction and the opening of the Amerasia Basin. In *Circum-Arctic Lithosphere Evolution* (eds V Pease and B Coakley), pp. 159–82. Geological Society of London, Special Publication no. 460.

Piepjohn K, Von Gosen W and Tessensohn F (2016) The Eurekan deformation in the Arctic: an outline. *Journal of the Geological Society, London* **173**, 1007–24.

Pugh AT, Schröder-Adams CJ, Carter ES, Herrle JO, Galloway J, Haggart JW, Andrews JL and Hatsukano K (2014) Cenomanian to Santonian radiolarian biostratigraphy, carbon isotope stratigraphy and paleoenvironments of the Sverdrup Basin, Ellef Ringnes Island, Nunavut, Canada. *Palaeogeography, Palaeoclimatology, Palaeoecology* **413**, 101–22.

Ricketts B, Osadetz KG and Embry AF (1985) Volcanic style in the Strand Fiord Formation (Upper Cretaceous), Axel Heiberg Island, Canadian Arctic Archipelago. *Polar Research* **3**, 107–22.

Ricketts BD (1986) New formations in the Eureka Sound Group, Canadian Arctic Islands. *Geological Survey of Canada, Current Research, Part B, Paper 86-1B*, 363–74.

Ricketts BD (1991) Delta evolution in the Eureka Sound Group, western Axel Heiberg Island: the transition from wave-dominated to fluvial-dominated deltas. *Geological Survey of Canada, Bulletin* **402**, 1–72.

Ricketts BD (1994) *Basin Analysis, Eureka Sound Group, Axel Heiberg and Ellesmere Islands, Canadian Arctic Archipelago*. Geological Survey of Canada, Memoir 439, 119 pp.

Rudnick RL and Gao S (2003) Composition of the continental crust. In *Treatise on Geochemistry* (eds HD Holland and KK Turekian), pp. 1–64. Oxford: Pergamon.

Saumur BM, Dewing K and Williamson MC (2016) Architecture of the Canadian portion of the High Arctic Large Igneous Province and implications for magmatic Ni–Cu potential. *Canadian Journal of Earth Sciences* **53**, 528–42.

Schandl ES and Gorton MP (2002) Application of high field strength elements to discriminate tectonic settings in VMS environments. *Economic Geology* **97**, 629–42.

Schoene B, Crowley JL, Condon DJ, Schmitz MD and Bowring SA (2006) Reassessing the uranium decay constants for geochronology using ID-TIMS U–Pb data. *Geochimica et Cosmochimica Acta* **70**, 426–45.

Schröder-Adams CJ, Herrle JO, Embry AF, Haggart JW, Galloway JM, Pugh AT and Harwood DM (2014) Aptian to Santonian foraminiferal biostratigraphy and paleoenvironmental change in the Sverdrup Basin as revealed at Glacier Fiord, Axel Heiberg Island, Canadian Arctic Archipelago. *Palaeogeography, Palaeoclimatology, Palaeoecology* **413**, 81–100.

Sell BK, Samson SD, Mitchell CE, McLaughlin PI, Koenig AE and Leslie SA (2015) Stratigraphic correlations using trace elements in apatite from Late Ordovician (Sandbian–Katian) K-bentonites of eastern North America. *Geological Society of America Bulletin* **127**, 1259–74.

Snow CA (2006) A reevaluation of tectonic discrimination diagrams and a new probabilistic approach using large geochemical databases: moving beyond binary and ternary plots. *Journal of Geophysical Research: Solid Earth* **111**, B06206. doi: 10.1029/2005JB003799.

Souther JG (1963) Geological transverse across Axel Heiberg Island from Buchanan Lake to Strand Fiord. In *Geology of the North-Central Part of the Arctic Archipelago, Northwest Territories (Operation Franklin)* (ed. YO Fortier), pp. 426–48. Geological Survey of Canada, Memoir 320.

Spears DA, Kanaris-Sotiriou R, Riley N and Krause P (1999) Namurian bentonites in the Pennine Basin, UK – origin and magmatic affinities. *Sedimentology* **46**, 385–401.

Spicer RA and Herman AB (2010) The Late Cretaceous environment of the Arctic: a quantitative reassessment based on plant fossils. *Palaeogeography, Palaeoclimatology, Palaeoecology* **295**, 423–42.

Stacey, JS and Kramers, JD (1975) Approximation of terrestrial lead isotope evolution by a two-stage model. *Earth and Planetary Science Letters* **26**, 207–21.

Steiger RH and Jäger E (1977) Subcommission on geochronology: convention on the use of decay constants in geo- and cosmochronology. *Earth and Planetary Science Letters* **36**, 359–62.

Tapia PM and Harwood DM (2002) Upper Cretaceous diatom biostratigraphy of the Arctic Archipelago and northern continental margin, Canada. *Micropaleontology* **48**, 303–42.

Tarduno JA, Brinkman DB, Renne PR, Cottrell RD, Scher H and Castillo P (1998) Evidence for extreme climatic warmth from Late Cretaceous Arctic vertebrates. *Science* **282**, 2241–3.

Tegner C, Storey M, Holm PM, Thorarinsson SB, Zhao X, Lo CH and Knudsen MF (2011) Magmatism and Eurekan deformation in the High Arctic Large Igneous Province: ^{40}Ar–^{39}Ar age of Kap Washington Group volcanics, North Greenland. *Earth and Planetary Science Letters* **303**, 203–14.

Thórarinsson SB, Holm PM, Tappe S, Heaman LM and Tegner C (2011) Late Cretaceous–Palaeocene continental rifting in the High Arctic: U–Pb geochronology of the Kap Washington Group volcanic sequence, North Greenland. *Journal of the Geological Society, London* **168**, 1093–106.

Thórarinsson SB, Söderlund U, Døssing A, Holm PM, Ernst RE and Tegner C (2015) Rift magmatism on the Eurasia basin margin: U–Pb baddeleyite ages of alkaline dyke swarms in North Greenland. *Journal of the Geological Society, London* **172**, 721–6.

Tikhomirov PL, Kalinina EA, Kobayashi K and Nakamura E (2008) Late Mesozoic silicic magmatism of the North Chukotka area (NE Russia): age, magma sources, and geodynamic implications. *Lithos* **105**, 329–46.

Tikhomirov PL, Kalinina EA, Moriguti T, Makishima A, Kobayashi K, Cherepanova IY and Nakamura E (2012) The Cretaceous Okhotsk–Chukotka Volcanic Belt (NE Russia): geology, geochronology, magma output rates, and implications on the genesis of silicic LIPs. *Journal of Volcanology and Geothermal Research* **221–222**, 14–32.

Tozer ET (1963) Mesozoic and Tertiary stratigraphy. In *Geology of the North Central Part of the Arctic Archipelago, Northwest Territories (Operation Franklin)* (ed. YO Fortier), pp. 74–100. Geological Survey of Canada, Memoir 320.

Tozer ET and Thorsteinsson R (1964) *Western Queen Elizabeth Islands, Arctic Archipelago*. Geological Survey of Canada, Memoir 332, 242 pp.

Trettin HP (1996) *Chemical Analyses of Upper Cretaceous Volcanics and Related(?) Sills, Northwestern Ellesmere Island, District of Franklin*. Geological Survey of Canada, Open File 3274, 30 pp.

Trettin HP and Parrish R (1987) Late Cretaceous bimodal magmatism, northern Ellesmere Island: isotopic age and origin. *Canadian Journal of Earth Sciences* **24**, 257–65.

Tullius DN, Leier AL, Galloway JM, Embry AF and Pedersen PK (2014) Sedimentology and stratigraphy of the Lower Cretaceous Isachsen Formation: Ellef Ringnes Island, Sverdrup Basin, Canadian Arctic Archipelago. *Marine and Petroleum Geology* **57**, 135–51.

Vavrek MJ, Hills LV and Currie PJ (2014) A hadrosaurid (Dinosauria: Ornithischia) from the Late Cretaceous (Campanian) Kanguk Formation of Axel Heiberg Island, Nunavut, Canada, and its ecological and geographical implications. *Arctic* **67**, 1–9.

Villeneuve M and Williamson M-C (2006) ^{40}Ar–^{39}Ar dating of mafic magmatism from the Sverdrup Basin magmatic province. In Proceedings of the Fourth International Conference on Arctic Margins (ICAM IV), 30 September – 3 October 2003, Dartmouth, Nova Scotia (eds RA Scott and DK Thurston), pp. 206–15.

Wang P and Glover L (1992) A tectonics test of the most commonly used geochemical discriminant diagrams and patterns. *Earth-Science Reviews* **33**, 111–31.

Wark DA and Miller CF (1993) Accessory mineral behavior during differentiation of a granite suite: monazite, xenotime and zircon in the Sweetwater Wash pluton, southeastern California, U.S.A. *Chemical Geology* **110**, 49–67.

Watson EB (1979) Zircon saturation in felsic liquids: experimental results and applications to trace element geochemistry. *Contributions to Mineralogy and Petrology* **70**, 407–19.

Weaver C (1963) Interpretative value of heavy minerals from bentonites. *Journal of Sedimentary Research* **33**, 343–49.

Wheeler JO, Brookfield AJ, Gabrielse H, Monger JWH, Tipper HW and Woodsworth GJ (1991) *Terrane Map of the Canadian Cordillera. 'A' Series Map, 1713A*. Ottawa: Geological Survey of Canada.

Whitehouse MJ and Kamber BS (2005) Assigning dates to thin gneissic veins in high-grade metamorphic terranes: a cautionary tale from Akilia, southwest Greenland. *Journal of Petrology* **46**, 291–318.

Wiedenbeck M, Allé P, Corfu F, Griffin WL, Meier M, Oberli F, Quadt AV, Roddick JC and Spiegel W (1995) Three natural zircon standards for U–Th–Pb, Lu–Hf, trace element and REE analyses. *Geostandards Newsletter* **19**, 1–23.

Winchester JA and Floyd PA (1977) Geochemical discrimination of different magma series and their differentiation products using immobile elements. *Chemical Geology* **20**, 325–43.

Witkowski J, Harwood DM and Chin K (2011) Taxonomic composition, paleoecology and biostratigraphy of Late Cretaceous diatoms from Devon Island, Nunavut, Canadian High Arctic. *Cretaceous Research* **32**, 277–300.

Wray DS (1995) Origin of clay-rich beds in Turonian chalks from Lower Saxony, Germany — a rare-earth element study. *Chemical Geology* **119**, 161–73.

Zielinski RA (1982) The mobility of uranium and other elements during alteration of rhyolite ash to montmorillonite: a case study in the Troublesome Formation, Colorado, U.S.A. *Chemical Geology* **35**, 185–204.